Decoding the North Atlantic Ocean Circulation Breakthrough in the Aptian–Albian Transition

João. M. F. Ramos [1,2], Jairo. F. Savian [1,3], Daniel. R. Franco [4], Milene F. Figueiredo [5], Rodolfo Coccioni [6], Fabrizio Frontalini [7]

[1]Programa de Pós-Graduação em Geociências, Instituto de Geociências, Universidade Federal do Rio Grande do Sul, Av. Bento Gonçalves 9500, 91501-970 Porto Alegre, RS, Brazil.
[2]Petróleo Brasileiro S.A., Rio de Janeiro (PETROBRAS), Av. Henrique Valadares 28, 20231-030 - Rio de Janeiro- RJ, Brazil.
[3]Instituto de Geociências, Universidade Federal do Rio Grande do Sul, Av. Bento Gonçalves 9500, 91501-970 Porto Alegre, RS, Brazil.
[4]Coordenação de Geofísica, Observatório Nacional, R. General José Cristino 77, 20921-400 Rio de Janeiro, RJ, Brazil.
[5]Centro de Pesquisas e Desenvolvimento Leopoldo Américo Miguez de Mello, Petrobras Petróleo Brasileiro S.A, Avenida Horácio Macedo 950, 21941-915 Rio de Janeiro, Brazil.
[6]Università degli Studi di Urbino "Carlo Bo", 61029 Urbino, Italy.
[7]Dipartimento di Scienze Pure e Applicate (DiSPeA), Università degli Studi di Urbino "Carlo Bo", 61029 Urbino, Italy.

Correspondence to: João Mauricio Figueiredo Ramos (j.m.f.ramos@petrobras.com.br)

Abstract. The Cretaceous experienced marked climatic variability driven by large igneous province volcanism, monsoonal dynamics and changes in ocean circulation, which strongly influenced the expression of oceanic anoxic events and Cretaceous Oceanic Red Beds (CORBs). Here we integrate cyclostratigraphic analysis of magnetic susceptibility records from Ocean Drilling Program Site 1049 (western North Atlantic) to evaluate the timing and synchronicity of CORB deposition between the Tethyan and North Atlantic realms. Our results show that long-lived Aptian CORBs coincided with global cooling and enhanced thermohaline circulation, whereas Albian CORBs were shorter lived and orbitally paced, reflecting greenhouse conditions dominated by circulation driven primarily by mesoscale eddies. Astrochronological tuning further constrains two short geomagnetic polarity reversals within the Cretaceous Normal Polarity Superchron, dating the M–2r reversal to 110.76 Ma (duration ~150 kyr) and placing reversed-polarity subchron 3 between 111.45 and 111.53 Ma. These ages provide robust geochronological tie points for Aptian–Albian stratigraphic correlations.~~The Aptian–Albian interval was marked by significant climatic changes driven by intense volcanism, monsoonal activity, and shifts in ocean circulation, which influenced sedimentary expression of oceanic anoxic events (OAEs) and Cretaceous oceanic red beds (CORBs). The formation of CORBs was primarily influenced by oxygen flux, sea-level changes, and atmospheric dust, with thermohaline circulation playing a key role in deep-water oxygenation. This study combines magneto-cyclostratigraphic analyses from Ocean Drilling Program (ODP) Site 1049 to assess the temporal synchrony of CORB-related events between the Tethys and North Atlantic. The results~~

provide new insights into CORB formation and paleoclimatic conditions during the Aptian–Albian interval. The onset of long-term Aptian CORBs is linked to global cooling and intensified thermohaline circulation, while Albian CORBs exhibit shorter, cyclic deposition influenced by orbital forcing. Orbital tuning of short geomagnetic reversals at ODP Site 1049 reveals that the M-2r reversal occurred at 110.76 Ma with a timespan of 150 kyr, and the reversed-polarity subchron "3" was between 111.45 and 111.53 Ma, which represent important tie points for geochronological models of Aptian–Albian interval.

1 Introduction

The Aptian–Albian interval (121.4 - 100.5 Ma; Ogg Gale et al., 2020) was marked by climatic shifts and extremely warm climate (Savin, 1977; Weissert, 1989; McAnena et al., 2013; Huber et al., 2018), which was much warmer than that of today (Friedrich et al., 2012; O'Brien et al., 2017; Huber et al., 2018). These significant paleoclimatic shifts driven by intense volcanism associated with the emplacement of large igneous provinces (LIPs) ((Schlanger and Jenkyns, 1976; Tarduno et al., 1991; Larson and Erba, 1999; Schlanger & Jenkyns, 1976; Tarduno et al., 1991; Percival et al., 2024; Li et al., 2024), elevated production of ocean crust (Larson, 1991), enhanced monsoonal activity (Matsumoto et al., 2022), and changes in oceanic circulation (Weissert, 1981; Premoli Silva et al., 1989; Hay, 2008, 2009; Larson, 1991; Giorgioni et al., 2015; Bottini and Erba, 2018; Gale et al., 2020; Matsumoto et al., 2022; Ramos et al., 2024a). These fluctuations played a crucial role in shaping the sedimentary record, contributing to both the deposition of organic-rich black shales which, with different definitions, are known in the literature as oceanic anoxic events (OAEs; Schlanger and Jenkyns, 1976, Leckie et al., 2002); Arthur et al., 1990; Coccioni et al., 2012, 2014) and the formation of Cretaceous oceanic red beds (CORBs), which signal episodes of improved oceanic oxygenation (Premoli Silva et al., 1989; Erbacher et al., 20112001; Wang et al., 2009; Li et al., 2011; Hu et al., 2012).

CORBs are fine-grained sedimentary rocks exhibiting red, pink, or brown hues, which are deposited in oxygen-rich pelagic marine settings (Hu et al., 2005a,b; Wang et al., 2005; Li et al., 2011). Their coloration is primarily attributed to iron oxides such as hematite and goethite, formed via syn-depositional oxidation and influenced by early diagenetic processes (Channell et al., 1982; Eren and Kadir, 2001; Li et al., 2011). Based on XRD and diffuse reflectance spectrophotometry (DRS) analyses, Hu et al. (2006b) proposed that the red coloration of the ODP Site1049 sediments could be attributed to the presence of microscopic, finely dispersed hematite. The widespread presence of benthic foraminifera in CORBs suggests oligotrophic and oxic bottom-water conditions and shifts in their assemblages from dysoxic to oxic states further reflect stepwise improvements in ocean ventilation during their deposition (Erbacher et al., 2001; Wang et al., 2009; Kochhann et al., 2023).

Whereas OAE deposition has been linked to an intensified hydrological cycle and reduced vertical mixing (Fischer and Arthur, 1977; Sinninghe Damsté and Köster, 1998; Erbacher et al., 2001; Matsumoto et al., 2022), CORB formation reflects contrasting environmental conditions, characterized by increased aridity, enhanced input of iron-rich aeolian dust, and

Formatado: Não Realce

Formatado: Não Realce

intensified vertical mixing and bottom-current activity that promoted water-column ventilation and oxygenation ~~While the deposition of OAEs has been linked to an intensified hydrological cycle and reduced vertical mixing in the water column (Fisher and Arthur, 1977; Sinninghe Damsté and Köster, 1998; Erbacher et al., 2001; Matsumoto et al., 2022), the formation of CORBs appears to be associated with contrasting environmental conditions, such as periods of aridity, increased delivery of aeolian iron-rich dust, and enhanced vertical mixing and ventilation of the water column~~ (Hu et al., 2012; Giorgioni et al., 2017). Although the periodic influx of cooler deep waters is considered a key driver in CORB formation (Hu et al., 2005b), multiple factors may have contributed to the formation of CORBs (e.g., oxygen flux into pore waters, prolonged oxygen exposure, changes in sea level, basin geometry, organic matter content, and atmospheric dust fluxes; Hu et al., 2005a,b; Li et al., 2011; Hu et al., 2012), hence suggesting a complex and multifactorial origin for these deposits.

Among the proposed mechanisms for CORB formation, the presence of oxygenated bottom waters is considered the primary prerequisite for organic matter oxidation and the associated early diagenetic processes that characterize CORBs (Wang et al., 2009; Jansa and Hu, 2009). In this context, thermohaline circulation is widely recognized as the dominant mechanism responsible for deep-ocean oxygenation (Yamamoto et al., 2015). A fundamental requirement for the establishment of such circulation is the existence of strong latitudinal temperature gradients between cold polar regions and warm equatorial zones (Hay, 2008)—a condition generally considered atypical for the Cretaceous.

However, multiple lines of evidence indicate the occurrence of cooling events during the Aptian, despite the prevailing greenhouse climate, which may have enabled the development of a thermohaline circulation capable of modifying water-column stratification and promoting the oxidation of iron-bearing sediments in the presence of more oxygenated bottom waters (Hu et al., 2005a,b; Tiraboschi et al., 2009; Erbacher et al., 2001; Li et al., 2011; McAnena et al., 2013;). Accordingly, a link between CORB deposition and thermohaline circulation can be proposed for the Aptian Cold Snap (McAnena et al., 2013). Nevertheless, CORB occurrence is not restricted to the late Aptian. In the Tethyan realm, CORBs span from the Aptian to the Albian (Premoli Silva et al., 1989; Coccioni et al., 2012; Gambacorta et al., 2016), encompassing both typical Cretaceous greenhouse conditions and cooler interludes. A similar pattern is observed in the North Atlantic, where CORBs occur over the same time interval (Erbacher et al., 2001; Trabucho Alexandre et al., 2011; Li et al., 2011). The geochemical characteristics of these red beds, together with the duration of oxidation events across contrasting thermal regimes, likely hold key insights into Aptian–Albian paleoclimate evolution and ocean circulation modes.

~~Dentre todas as possíveis causas da formação dos CORBs, a presença de águas de fundo oxigenadas é pontuada como a condição primordial, onde a Thermohaline circulation provavelmente desempenha um papel crucial, já que is widely recognized as the primary mechanism for deep-sea oxygenation (Yamamoto et al., 2015). Adicionalmente, esse tipo de circulação é amplificada em períodos em que existam contraste de temperatura entre as regiões polares e equatoriais (refs).~~

~~Cooling events during the Aptian – despite an overarching greenhouse climate – have been shown to affect water column stratification, enabling oxidation of iron-bearing sediments in the presence of more oxygenated bottom waters (McAnena et al., 2013; Tiraboschi et al., 2009; Erbacher et al., 2011; Hu et al., 2005a,b; Li et al., 2011).~~

Formatado: Fonte: Não Negrito

Formatado: Inglês (Estados Unidos)

~~Assim, uma correspondência entre a presença dos CORBs e a Thermohaline circulation pode ser sugerida, dando erroneamente a sugestão de que a ocorrência dos CORBs estaria limitada ao intervalo do Cold Snap Aptiano (McAnena et al., 2013). In the Tethyan realm, CORBs occurrence are spread on Aptian and Albian times, both at The typical Cretaceous greenhouse conditions and also at the Aptian cooling interlude known as cold snap (McAnena et al., 2013), e as durações desses eventos em ambos os regimes de temperature could be the the key to deciphering the Aptian/Albian paleoclimate.~~

~~In the absence of widespread thermohaline circulation, other regional processes may facilitate oxygenation of bottom waters, including local ventilation (Ahmerkamp et al., 2017), turbulent vertical mixing (Dossmann et al., 2017), episodic events like storms or cyclones (Rovelli et al., 2016), reduced biological oxygen demand (Wang et al., 2020), and surface-water cooling (Fearon et al., 2020). These mechanisms tend to be spatially constrained, indicating that orbitally forced CORBs might not be synchronous across all basins. Therefore, CORB deposition over intervals longer than Milankovitch cycles can yield valuable insights into deep-sea ocean circulation and long-term climatic stability.~~

In such context, the Ocean Drilling Program (ODP) Leg 171B, Site 1049, located at Blake Nose in the western North Atlantic, provides a unique opportunity to study short-term CORBs that appear to be orbitally-controlled (Ogg and Bardot, 2001). These CORB intervals are marked by distinctive sediment coloration and high magnetic susceptibility (MS) readings due to hematite presence (Li et al., 2011; Hu et al., 2012). Shipboard indications of two thin reversed-polarity zones in Holes from ODP Site 1049 (Norris et al., 1998) were later confirmed by Ogg and Bardot (2001), providing well-dated geomagnetic reversals based on global bioevents (Huber et al., 2011).

This study presents a magneto-cyclostratigraphic analysis based on spliced MS records from Holes A, B, and C of the ODP Site 1049 (Norris et al., 1998). The excellent preservation of planktonic foraminifera at this site (Erbacher et al., 2001) allows for precise dating of CORB intervals, as well as the estimation of sedimentation rates and durations. Astrochronological age models enable the temporal correlation of geological events across sedimentary basins, linking records from classical sections studied using different methodologies and deposited in distinct oceanic settings, such as ODP Site 1049 in the North Atlantic and the Poggio Le Guaine (PLG) section in the Tethyan realm.

By integrating orbital-cycle tuning of the MS dataset, the ages of short geomagnetic polarity reversals were constrained and updated in accordance with the latest Aptian–Albian biochronologies (Gale et al., 2020) and the ages of the key features of the carbon isotope curves (Ramos et al., 2024a,b). These reversals were subsequently correlated with other known events recorded during the Cretaceous Normal Superchron (CNPS) in multiple global locations (Baksi, 1995; Tarduno, 1990; Gilder et al., 2003; Zhang et al., 2021; Fauth et al., 2022; Ramos et al., 2024b). Our results provide new insights into the paleoclimate of the Aptian–Albian interval and offer a comprehensive review of the key mechanisms related to CORB formation under different circulation modes.~~Our results provide new insights into the geochronology of the Aptian–Albian interval to better understanding the CORBs.~~

2 Geological setting

The Blake Nose, located in the western North Atlantic (Fig.~~ure~~ 1), resembles an appendage on the eastern margin of the Blake Plateau, a gently sloping ramp that reaches a maximum depth of about 2700 m (Norris et al., 1998; Li et al., 2011). The Upper Cretaceous and Cenozoic deposits on the Blake Nose lie upon a sequence of Jurassic and Lower Cretaceous limestone ~~(Benson et al., 1978)~~. ODP Leg 171B drilled five ~~holes~~ sites along the Blake Nose transect, and three holes were drilled at Site 1049, positioned at 23°N during the Cretaceous, above the calcite ~~carbonate~~ compensation depth (CCD).

The Cretaceous sediments at this site are primarily composed of nannofossil chalk, clayey nannofossil chalk, nannofossil clay, clay, and an organic-rich black shale (Norris et al., 1998)~~planktonic foraminifers, quartz, and clasts of limestone, dolomite, chalk, chert, and schist~~. The glassy shells of planktonic and benthic foraminiferal species suggest minimal diagenetic alteration (~~Norris et al., 1998;~~ Erbacher et al., 2001; Li et al., 2011). The sediments are clayey calcareous nannofossil-bearing chalk and claystone, rich in planktonic foraminiferal assemblages, with color variations in red, white, green, and black beds. Several intervals at different ~~sites of the Sites~~Holes 1049A, 1049B and 1049C display color and compositional oscillations that appear to reflect a spectrum of Milankovitch orbital climate cycles (Ogg and Bardot, 2001). The laminated black shale, associated with OAE 1b (Norris et al., 1998; Erbacher et al., 2001; Huber and Leckie, 2011), is located within the *M. rischi* planktonic foraminiferal zone and near the base of the *Hayesites albiensis* nannofossil zone, linking it to the Urbino/Paquier Level (Coccioni et al., 2012, 2014; Ramos et al., 2024a).

The color of oceanic red beds, influenced by hematite and goethite, reflects syn-depositional oxidation and early diagenesis, with no evidence of late diagenetic alteration (Wang et al., 2009; Li et al., 2011). ~~A~~ At ODP Site 1049, a consistent terrigenous input and a clay mineral assemblage typical of a dry, cold climate with low rainfall suggest that iron oxides formed under oxic bottom-water conditions (Wang et al., 2009). The presence of a flourishing benthic community (Norris et al., 1998; Kochhann et al., 2023) further supports this interpretation. These conditions were likely driven by low organic matter accumulation and high dissolved oxygen content in bottom waters (Li et al., 2011).

The Poggio Le Guaine (PLG) core, drilled in the Umbria–Marche Basin of central Italy, includes some of the most complete Aptian and Albian sedimentary successions known from the Tethyan Realm and provides the basis for an accurate and precise calibration of the Paleogene time scale (Coccioni et al., 2012; Leandro et al., 2022). The astrochronology performed on this core, based on magnetic susceptibility, provides the most detailed zonation of OAE 1b (and its sub-events), as well as the definition of the ages of the main features of the carbon-isotope curve associated with this anoxic event (Ramos et al., 2024a), sequenced using Greek letters (Fig. 3). These c-marks, due to the global nature of the carbon-related isotopic anomalies (Weissert, 1989), incorporate chemostratigraphic tie-points that enable long-distance correlations between successions in different sedimentary basins (Ramos et al., 2024a).

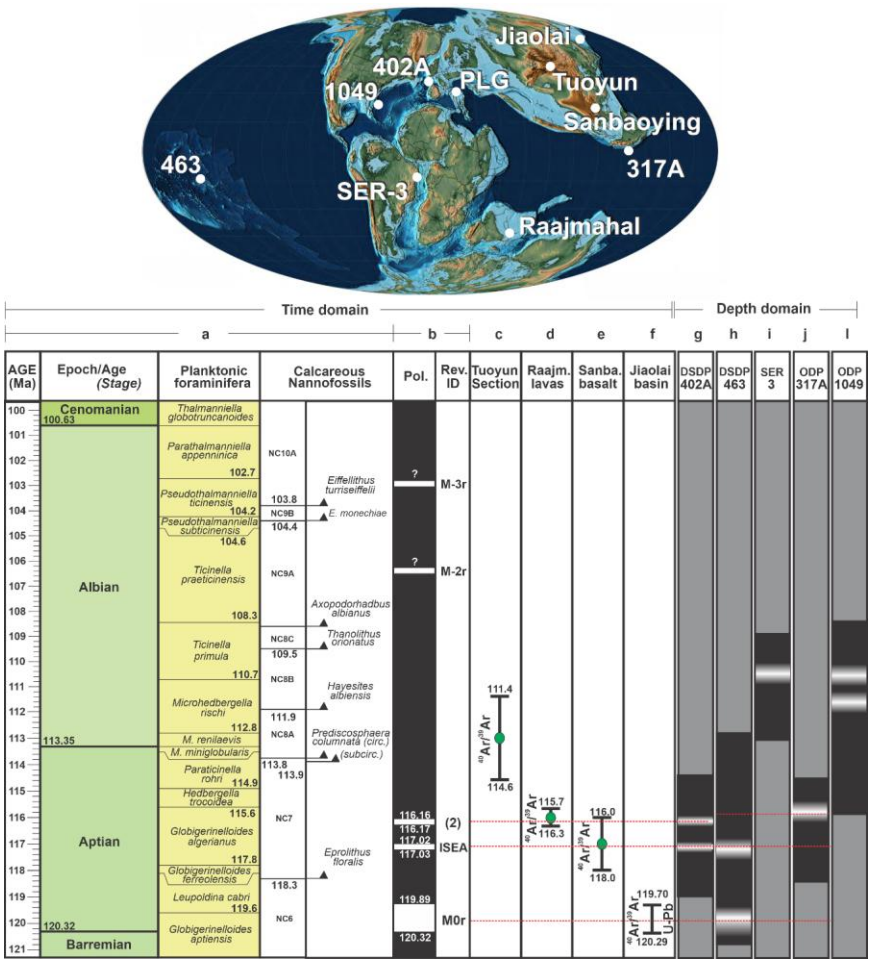

Figure 1: Top: Early Albian paleogeographic reconstructions at 110 Ma with the location of the ODP Site 1049, PLG core and the other sites/outcrops used for the short geomagnetic reversed-polarity correlations. Sea Level +80 m, Mollweide Projection. Modified from CR Scotese, PALEOMAP Project. Bottom: a) The stratigraphic framework with age (Ma), planktonic foraminiferal and calcareous nannofossils zones (Huber and Leckie, 2011; Coccioni et al., 2012; Gale et al., 2020; Ramos et al., 2024a,b). b) Geomagnetic polarity and reversal identifications (Savian et al., 2016; Gale et al., 2020; Li et al., 2023; Ramos et al., 2024b, 2025). c) Tuoyun section (Gilder et al., 2003). d) Raajmahal Traps (Baksi, 1995). e) Sanbaoying, Liaoning Province (Shi et al., 2004). f) Jiaolai Basin (Li et al., 2023). g) DSDP Site 402A (Tarduno, 1990; Ramos et al., 2024b). h) DSPDP Site 463 (Tarduno, 1990). i) SER-3 core (Fauth et al., 2022). J) ODP Site 317A (Tarduno, 1990). l) ODP Site 1049 (Ogg and Bardot, 2001).

3 Methods

All data used in this study (i.e., the MS dataset and the spliced instructions for cores from Holes 1049A [Core 19X, 1-4], 1049B [Core 11X, 1-2 and Core 12X, 1-5], and 1049C [Core 12X, 1-cc]) were obtained from the Laboratory Information Management System (LIMS) online repository of the International Ocean Discovery Program (available at https://web.iodp.tamu.edu/LORE/). Norris et al. (1998) provided a ODP Site 1049 spliced (~~Figure~~ Fig. 2d) ranging from 131.0 to 151.3 mbsf based on the shipboard low-field magnetic susceptibility (MS) data (measured on whole-round core sections at each 2 cm) from Holes A, B and C (Fig~~ure~~s. 2a to 2c, respectively), which was used for our cyclostratigraphic analyses. The ODP Site 1049 spliced comprises the upper section from Hole A (Cores 19X-1 to 19X-4), complemented by Hole B (Core 11X-1). From 138.28 mbsf to 146.03 mbsf, the Spliced Hole is constructed using Cores 12X-1 to 12X-6 from Hole C. Finally, the basal part of the Spliced Hole is composed using Cores 12X-1 to 12X-5 from Hole C (~~Figure~~ Fig. 2d). We constrained the magnetostratigraphic evaluation of Ogg and Bardot (2001) at the 144.0 – 160.5 mbsf interval from Hole 1049A, which exhibited the higher core recovery and comprises both the top Albian unconformity and the unconformity separating the Aptian-Albian intervals.

3.1 Magnetostratigraphy

As discussed above, a preliminary magnetostratigraphic framework for ODP Site 1049 was first presented by Norris et al. (1998) and subsequently reinterpreted through detailed paleomagnetic analyses of minicore suites using stepwise thermal demagnetization (Ogg and Bardot, 2001). These latter authors interpreted the upper Aptian reversed-polarity interval (~155 mbsf; 171B-1049A-20X-1) as a diagenetic artifact related to post-Albian iron mobilization driven by redox contrasts near an organic-rich horizon. However, a normally magnetized sample (20X-2, 30–32 cm) occurs between the questioned reversed interval and the underlying black shale. This sample displays pronounced yellowish and greenish staining in the original sediments, suggesting preservation of the primary magnetization.

Independent mineralogical and biostratigraphic evidence argues against significant late diagenetic overprinting at ODP Hole 1049C. Clay mineral assemblages show no systematic depth-related trends; notably, illite and chlorite do not progressively replace smectite with increasing burial depth, indicating the absence of burial diagenesis (Li et al., 2011). In addition, planktonic and benthic foraminifera exhibit glassy tests with well-preserved surface ornamentation and no calcite infilling, further supporting minimal diagenetic alteration (Erbacher et al., 2001; Li et al., 2011). The occurrence of goethite precisely at the level recording the older reversed geomagnetic field provides additional support that the magnetic mineralogy remained largely unmodified and did not overprint a younger reversed polarity signal (Li et al., 2011). Therefore, this reversal is retained as valid in our study.

Formatado: Inglês (Estados Unidos)
Formatado: Fonte: Não Itálico, Inglês (Estados Unidos)
Formatado: Inglês (Estados Unidos)
Formatado: Inglês (Estados Unidos)
Formatado: Fonte: Não Itálico, Inglês (Estados Unidos)
Formatado: Inglês (Estados Unidos)
Formatado: Fonte: Não Itálico, Inglês (Estados Unidos)
Formatado: Inglês (Estados Unidos)
Formatado: Fonte: Não Itálico, Inglês (Estados Unidos)
Formatado: Inglês (Estados Unidos)
Formatado: Fonte: Não Itálico, Inglês (Estados Unidos)
Formatado: Inglês (Estados Unidos)

Within the broader magnetostratigraphic context, Ryan et al. (1978) documented seven short-duration geomagnetic reversals during the Aptian–Albian interval, excluding M0r. The earliest of these was termed M-1r, whereas the second Aptian reversal, although listed in their Table 6 (see Ryan et al., 1978), was left unnamed. A third reversal, occurring in the Albian, was designated M-2r, followed by another unnamed event. The antepenultimate Albian reversal was termed M-3r, while the final two reversals also remained unnamed. Although commonly treated as isolated events (e.g., Gale et al., 2020), short reversals within the CNPS are frequently organized into closely spaced reversal sets (Ryan et al., 1978; Tarduno et al., 1992; Zhang et al., 2021; Ramos et al., 2025).

Using biostratigraphic constraints and an estimated inter-event spacing of ~860 kyr, Ramos et al. (2024b) subdivided the reversal traditionally referred to as M-1r (sensu Gale et al., 2020) into two distinct Lower Aptian events, termed M-1r and reversal “2”. This pair of reversals has been identified both at DSDP Site 402A in the eastern North Atlantic and within the Brazilian Equatorial Margin, with comparable timespans and inter-event intervals (Ramos et al., 2024b, 2025).

The reverse-polarity event defined as M-2r was likewise initially recognized as a pair of closely spaced reversals (Ryan et al., 1978; Tarduno et al., 1992), occurring within the *Prediscosphaera cretacea* or *Prediscosphaera columnata* biozones. Because reversal “2” of Ramos et al. (2024b) is constrained to the Aptian and stratigraphically underlies the reversed interval identified here, we designate this newly recognized short reversal as “3” (Fig. 2). A second reversed-polarity interval at ~146.5 mbsf (171B-1049A-19X-2, 103–105 cm) is interpreted as the Albian subchron M-2r and is recorded consistently in two holes at ODP Site 1049 (Fig. 2). For both reversals, upper and lower boundaries were defined at the intersections between the inclination-depth interpolation and the 0° inclination axis.

On this basis, we further subdivide the reversal previously assigned to M-2r (sensu Gale et al., 2020) into two discrete events, retaining the name M-2r for the younger reversal and assigning the older event to reversal “3”.

As discussed previously, a preliminary magnetostratigraphy study from ODP Site 1049 was presented by Norris et al. (1998), and the polarity intervals were later reinterpreted through paleomagnetic analyses of suites of minicores using stepwise thermal demagnetization (Ogg and Bardot, 2001). These authors characterized the upper Aptian reversed-polarity interval (~155 mbsf, 171B-1049A-20X-1, 121–123 cm) as a diagenetic artifact resulting from post-Albian iron mobilization induced by redox contrasts near this organic-rich interval. Nonetheless, a sample showing normal polarity (20X-2, 30-32, 202–30 cm) was found between the questioned reversed sample and the organic-rich black shale. This sample exhibited an even more anomalous yellowish and greenish staining in the original sediments, which preserved the initial magnetization. Therefore, this reversal is retained as valid in our study. Ryan et al. (1978) documented seven short reversals during the Aptian–Albian interval, excluding M0r. The earliest of these was designated M-1r. The second Aptian reversal, though listed in Table 6, was not named. The third reversal, occurring in the Albian, was labeled M-2r, followed by another unnamed event. The antepenultimate reversal of the Albian was termed M-3r, while the final two reversals remained unnamed. Based on biostratigraphic markers and an estimated time interval of approximately 860 kyr between reversal events, Ramos et al. (2024b) subdivided the M-1r reversal (as defined by Gale et al., 2020) into two distinct events, referred to as M-1r and “2”.Since reversal “2” (Ramos et al.,

Formatado: Inglês (Estados Unidos)
Formatado: Fonte: Não Itálico, Inglês (Estados Unidos)
Formatado: Inglês (Estados Unidos)
Formatado: Fonte: Não Itálico
Formatado: Inglês (Estados Unidos)
Formatado: Fonte: Não Itálico, Inglês (Estados Unidos)
Formatado: Inglês (Estados Unidos)
Formatado: Inglês (Estados Unidos)
Formatado: Fonte: Não Itálico, Inglês (Estados Unidos)
Formatado: Inglês (Estados Unidos)
Formatado: Fonte: Não Itálico, Inglês (Estados Unidos)
Formatado: Inglês (Estados Unidos)
Formatado: Fonte: Não Itálico, Inglês (Estados Unidos)
Formatado: Inglês (Estados Unidos)
Formatado: Fonte: Não Itálico, Inglês (Estados Unidos)
Formatado: Inglês (Estados Unidos)
Formatado: Fonte: Não Itálico, Inglês (Estados Unidos)
Formatado: Inglês (Estados Unidos)
Formatado: Fonte: Não Itálico, Inglês (Estados Unidos)
Formatado: Inglês (Estados Unidos)
Formatado: Fonte: Não Itálico, Inglês (Estados Unidos)
Formatado: Inglês (Estados Unidos)
Formatado: Fonte: Não Itálico, Inglês (Estados Unidos)
Formatado: Inglês (Estados Unidos)
Formatado: Fonte: Não Itálico, Inglês (Estados Unidos)
Formatado: Inglês (Estados Unidos)
Formatado: Fonte: Não Itálico, Inglês (Estados Unidos)
Formatado: Inglês (Estados Unidos)
Formatado: Fonte: Não Itálico, Inglês (Estados Unidos)
Formatado: Inglês (Estados Unidos)

2024b) was dated to the Aptian and stratigraphically positioned beneath the reversal in question, we designate this new short reversal as "3" (Figure 2). The second zone of reversed polarity, located at approximately 146.5 mbsf (171B-1049A-19X-2, 103–105cm), has been interpreted as the Albian subchron M″-2r″. This reversal is identified in two separate holes at ODP Site 1049 (Figure 2). The upper and lower boundaries of both reversals were defined at the intervals where the line interpolating the sample inclinations intersects the 0° inclination axis.

Although often described as isolated reversal events (Gale et al., 2020), the short reversals within the SNC are frequently interpreted as part of reversal sets (Ryan et al., 1978; Tarduno et al., 1992; Zhang et al., 2021). Ryan et al. (1978) documented seven short reversals during the Aptian–Albian interval, excluding M0r. The earliest of these was designated M-1r. The second Aptian reversal, though listed in Table 6, was not named. The third reversal, occurring in the Albian, was labeled M-2r, followed by another unnamed event. The antepenultimate reversal of the Albian was termed M-3r, while the final two reversals remained unnamed. Based on biostratigraphic markers and an estimated time interval of approximately 860 kyr between reversal events, Ramos et al. (2024b) subdivided the M-1r reversal (as defined by Gale et al., 2020) into two distinct events, referred to as M-1r and "2". Building on this framework, our study further subdivides the M-2r reversal (Gale et al., 2020), identifying two separate events, with the younger reversal designated as "3" and the upper event retaining the original name, M-2r.

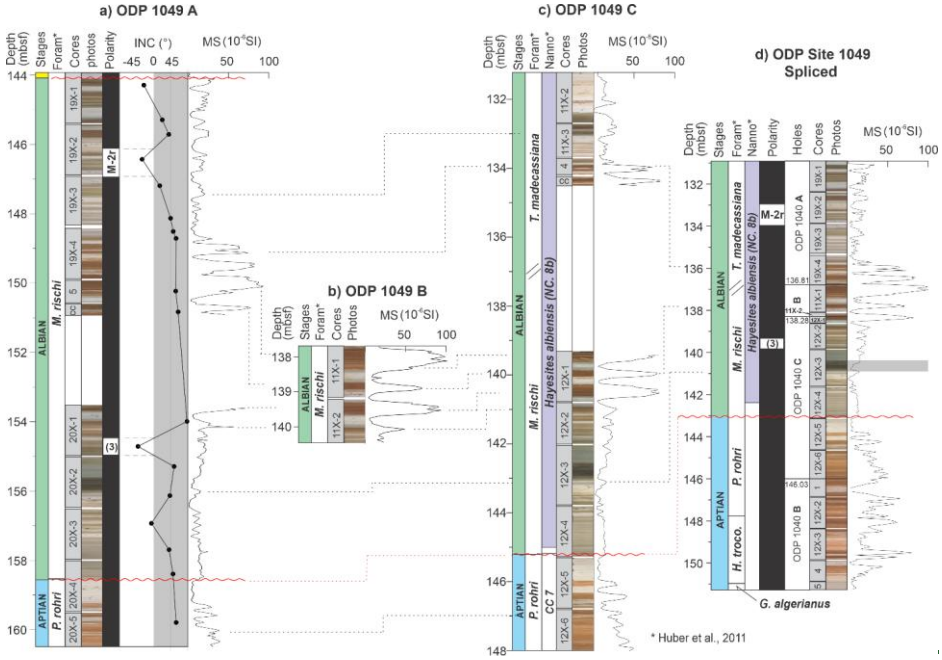

Figure 2: a) Magnetostratigraphy of ODP Site 1049 Hole A, showing planktonic foraminiferal zones (Huber et al., 2011), cores, core photographs, and geomagnetic polarity (Ogg and Bardot, 2001). b) Section of ODP Site 1049 Hole B used to compose the spliced section (Norris et al., 1998). c) Section of ODP Site 1049 Hole C. Planktonic foraminiferal and calcareous nannofossil zones from Huber et al. (2011). d) Spliced section of magnetic susceptibility data from Holes 1049A, 1049B, and 1049C (Norris et al., 1998). The magnetic polarity curve was derived from Hole A.

3.2 Cyclostratigraphy

Magnetic susceptibility, $CaCO_3$ and other geochemical records from the Aptian/Albian intervals (Li et al., 2011; Hu et al., 2022) show pronounced short-term cyclicity linked to Milankovitch forcing (Ogg and Bardot, 2001), reflecting alternations between phases of active water bottom circulation and episodes of water-column stagnation (Fig. 3). Cyclostratigraphic analysis of the ODP Site 1049 spliced was performed using version 2.4.1 of the Acycle software (Li et al., 2019). Due to the evenly spaced acquisition of the MS data, interpolation was not required. A locally weighted scatterplot smoothing ('lowess') trend of 3.97 m window (equivalent to ~20% of the entire data length) was removed prior to spectral analysis.

Formatado: Justificado

To investigate potential imprints of orbital forcing in the stratigraphy, spectral analyses were conducted using the multitaper method (MTM; Thompson, 1982) with two prolate tapers. Statistical significance was assessed by fitting a first-order autoregressive [AR(1)] red-noise null hypothesis and estimating confidence levels at 95% and 99%, following the robust background estimation procedure of Mann and Lees (1996). The transience and/or persistence of astronomical frequencies throughout the dataset was evaluated using Evolutive Harmonic Analysis (EHA; Meyers et al., 2001). Candidate orbital frequencies were then compared with those predicted by the La2004 astronomical solution for Aptian-Albian times (Laskar et al., 2004). Astronomical calibration was anchored on four tie points:

- **TP.1**: an age of 111.88 Ma for the base of the *H. albiensis* calcareous nannofossil Zone at 142.4 mcd, anchored between the c-markers ~~ιγ~~ and ~~ξe~~ (112.20 and 111.80 Ma, respectively) (Ramos et al., 2024a);
- **TP.2**: an age of 111.52 Ma for marker *o* at 139.5 mcd;
- **TP.3**: an age of 114.91 Ma for the first occurrence (FO) of the planktonic foraminifera *Paraticinella rohri* at 147.8 mcd; and
- **TP.4**: an age of 115.64 Ma for the FO of *Hedbergella trocoidea* at 153 mcd (Huber et al., 2011; Huber and Leckie, 2011; Ramos et al., 2024a,b) (~~Figure~~ Fig. 3).

Formatado: Fonte: 10 pt, Inglês (Estados Unidos), Verificar ortografia e gramática

Formatado: Recuo: À esquerda: 1 cm, Sem marcadores ou numeração

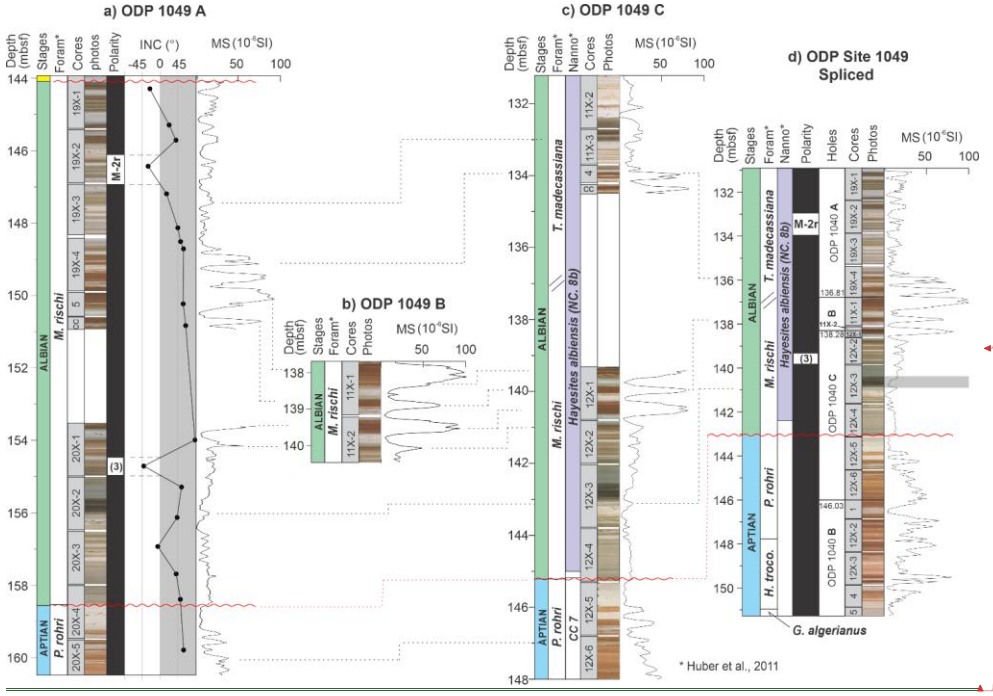

Figure 2: a) Magnetostratigraphy of ODP Site 1049 Hole A, showing planktonic foraminiferal zones (Huber et al., 2011), cores, core photographs, and geomagnetic polarity (Ogg and Bardot, 2001). b) Section of ODP Site 1049 Hole B used to compose the spliced section (Norris et al., 1998). c) Section of ODP Site 1049 Hole C. Planktonic foraminiferal and calcareous nannofossil zones from Huber et al. (2011). d) Spliced section of magnetic susceptibility data from Holes 1049A, 1049B, and 1049C (Norris et al., 1998). The magnetic polarity curve was derived from Hole A.

Formatado: Fonte: 10 pt, Inglês (Estados Unidos), Verificar ortografia e gramática

Formatado: Normal, Sem marcadores ou numeração

Formatado: Recuo: À esquerda: 1 cm, Sem marcadores ou numeração

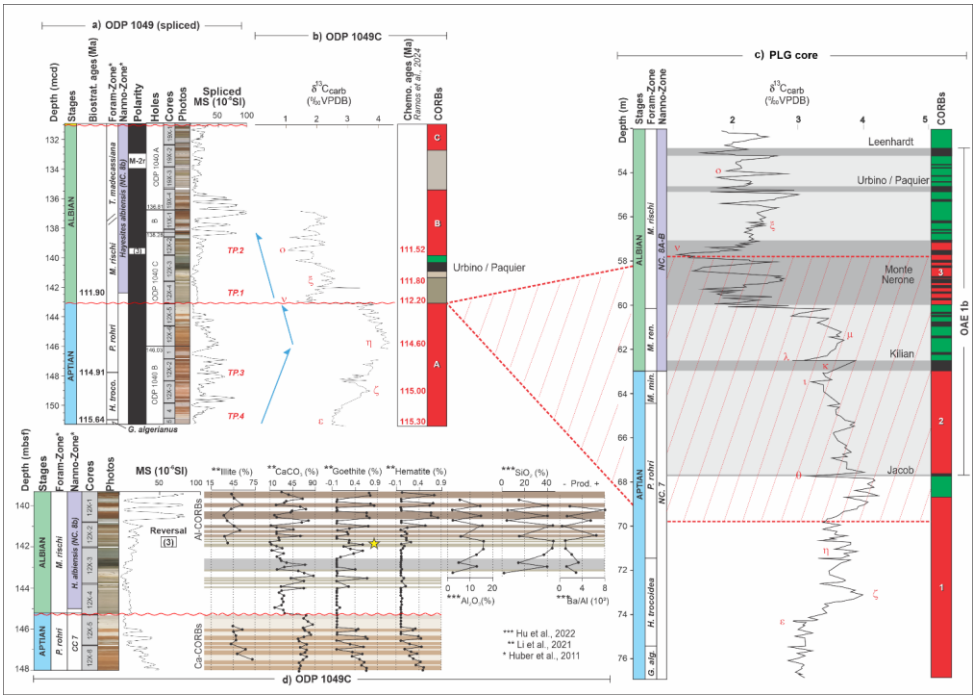

Figure 3: a) Magnetostratigraphy of ODP Site 1049 (spliced), showing planktonic foraminiferal zones (Huber et al., 2011), cores, core photographs, and geomagnetic polarity (Ogg and Bardot, 2001). Spliced section of magnetic susceptibility data from Holes 1049A, 1049B, and 1049C (Norris et al., 1998). The magnetic polarity curve was derived from Hole A. TP = tie-points. ~~Middle:~~b) Bulk carbonate samples from the upper Aptian–lower Albian interval of ODP Hole 1049C plotted alongside ages of the c-markers (Ramos et al., 2024a) and the CORBs levels. ~~Right:~~c) Correlated interval of the PLG core with stages, planktonic foraminiferal and calcareous nannofossil zones, bulk carbonate profile, c-markers, and CORBs numbers (Coccioni et al., 2012, 2014; Leandro et al., 2022). The shaded polygon represents the interval absent at ODP Site 1049. The grey square indicates the interval related to OAE 1b (Urbino/Paquier Level; Erbacher et al., 2001). d) Magnetic susceptibility and geochemical data (Li et al., 2011; Hu et al., 2012) from ODP Site 1049C, showing the cyclic variations between CORBs and non-CORBs intervals.

~~Left: Magnetostratigraphy of ODP Site 1049 (spliced), showing planktonic foraminiferal zones (Huber et al., 2011), cores, core photographs, and geomagnetic polarity (Ogg and Bardot, 2001). Spliced section of magnetic susceptibility data from Holes 1049A, 1049B, and 1049C (Norris et al., 1998). The magnetic polarity curve was derived from Hole A. TP = tiepoints. Middle: Bulk carbonate samples from the upper Aptian–lower Albian interval of ODP Hole 1049C plotted alongside ages of the c-markers (Ramos et al., 2024b) and the CORBs levels. Right: Correlated interval of the PLG core with stages, planktonic foraminiferal and calcareous nannofossil zones, bulk carbonate profile, c-markers, and CORBs numbers (Coccioni et al., 2012, 2014; Leandro et al., 2022; Ramos et al., 2024). The shaded polygon represents the interval eroded at ODP Site 1049. The grey square indicates the interval related to OAE 1b.~~

Formatado: Inglês (Reino Unido)

Formatado: Normal

4 Results

An unconformity separating the Aptian and Albian intervals at ODP Site 1049 was previously reported (Huber et al., 2011; Huber and Leckie, 2011; Hu et al., 2012). The identification of orbital imprints in the MS data was carried out independently for each interval. MTM spectral analyses of the MS records (~~Figure~~ Fig. 4a,d) revealed a broad spectral content, commonly exceeding the 95%–99% confidence thresholds (~~Figure~~ Fig. 4b,e). At the Aptian section, a sequence of spectral peaks compatible to the orbital imprint was identified with ratios of 256:83:62:23:14 cm = 18.3:5.9:4.4:1.6:1. These values closely align with the expected Milankovitch cyclicity for the Aptian (405:125:95:39:23 = 17.6:5.4:4.1:1.7:1; Waltham, 2015). Similarly, a set of spectral peaks for~~at~~ the Albian interval (357:128:97:34:18:15 cm) corresponds to a ratio of 23.8:8.5:6.5:2.3:1.2:1, which is in strong agreement with the predicted astronomical frequencies (405:125:95:39:23:18 = 22.5:6.9:5.3:2.2:1.3:1; Waltham, 2015).

Such findings indicate that the correspondence between observed and theoretical periodicities for both intervals suggests that sedimentation at ODP Site 1049 during the Aptian–Albian was likely influenced by orbital forcing, supporting earlier interpretations by Ogg and Bardot (2001). Additionally, analysis of both the power spectra and EHA results (~~Figure~~ Fig. 4c,f) revealed a low wavelength range pattern compatible to the orbital imprint which is quite stable throughout the studied interval. For the Aptian interval, we associated the following spectral bands with eccentricity signals: 405-kyr and 125/95-kyr, corresponding to 0.1–0.5 and 0.7–1.8 cycles/m, respectively. Additionally, we attributed the spectral bands of 2.2–4.6 m and greater than 5.2 cycles/m to the obliquity (~51 to ~29 kyr) and precession (~23 to ~14 kyr) signals, respectively (~~Figure~~ Fig. 4b,c). In the Albian interval, we related the following spectral bands with eccentricity signals: 405-kyr and 125/95-kyr, corresponding to 0.1–0.6 and 0.8–3.0 cycles/m, respectively. Similarly, the obliquity (~51 to ~29 kyr) and precession (~23 to ~14 kyr) signals were linked to the spectral bands of 3.6–6.4 and greater than 6.8 cycles/m, respectively (~~Figure~~ Fig. 4e,f). The interpreted 405-kyr long-eccentricity sinusoidal component was extracted from the MS record of ODP Site 1049 through Gaussian filtering, following the methodology outlined by Li et al. (2019). In our analysis, we correlated the minimum eccentricity phases derived from astronomical models (Laskar et al., 2004) with the lowest MS values in the dataset (~~Figure~~ Fig. 5a). After anchoring the stratigraphic positions of the tie points—TP.1 at 111.88 Ma, TP.2 at 111.52 Ma (located in close proximity to the reversal-polarity event "3"), TP.3 at 114.91 Ma, and TP.4 at 115.64 Ma—we estimated sediment accumulation rates (SARs) ranging between 0.4 and 0.8 cm/kyr (~~Figure~~ Fig. 5b).

Our astronomical tuning provided an age of ~ 111.45 Ma for the onset of reversal-polarity event "3", located at a depth of 139.5 mcd and spanning an estimated duration of ~80 kyr. Furthermore, an age of 110.61 Ma was assigned for the base of the M-2r reversed interval (~134 mcd) (Figs~~ures~~ ~~3c~~ 5c and ~~3d~~5d). We also constrained the age of the black shale interval—interpreted as a time equivalent of the Urbino Level (Coccioni et al., 2014; Ramos et al., 2024a)—to between 111.59 and 111.66 Ma. Additionally, the stratigraphic gap (Huber et al., 2011) represented by the unconformity was estimated to span approximately 2.56 million years.

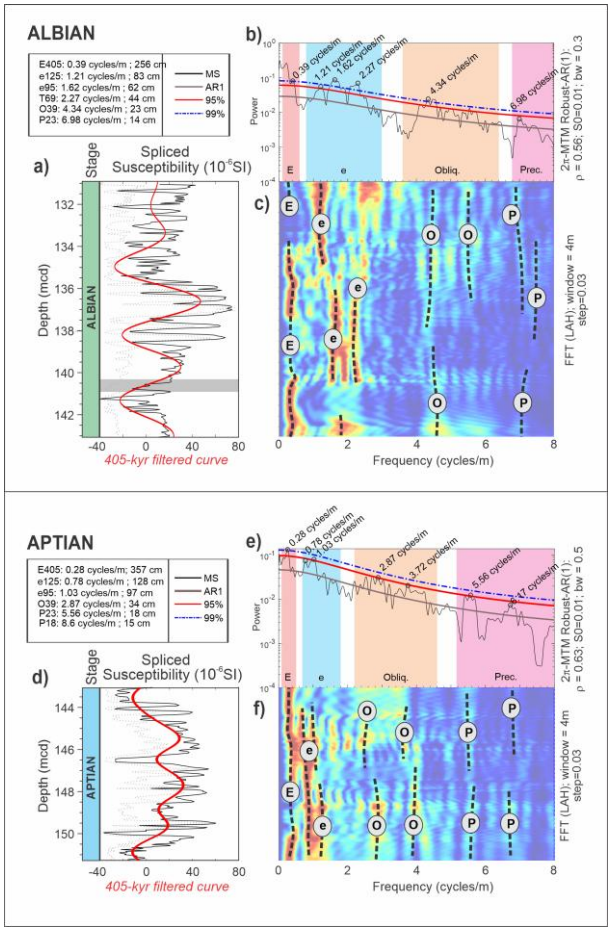

Figure 4: MS dataset prior and after Lowess detrending from the Albian (a) and Aptian (d) interval ODP Site 1049. Gray line: original MS values; black line: detrended MS data; red line: 405-kyr long eccentricity component. (b, e) Multitaper spectral estimator-based spectral analysis showing the interpreted cycles and the respective bands (colored rectangles). (c, f) evolutionary spectral analysis of series. E: long-eccentricity; e: short-eccentricity; Obliq: obliquity; Prec: precession index.

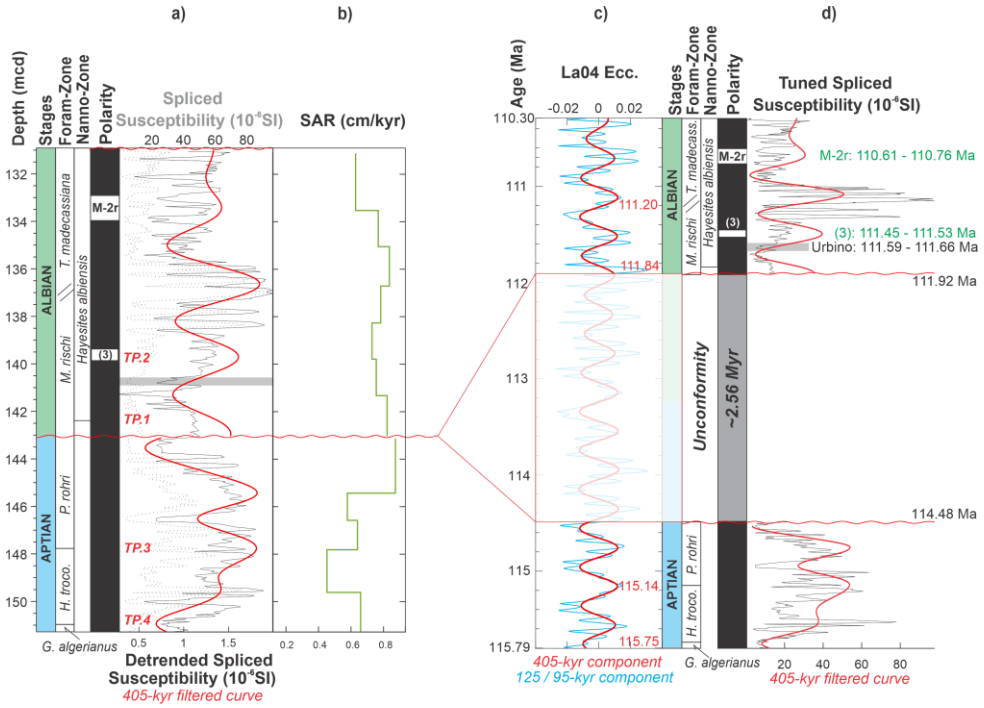

Figure 5: (a) Spliced MS (dashed grey line) and Lowess detrended MS (black line) and 405-kyr component (red line) of ODP Site 1049, presenting the stages, planktonic foraminifera and calcareous nannofossils zones, and geomagnetic polarity. TP.=tiepoint. b) SAR resulting from the tuning. c) Eccentricity signal from the La2004 astronomical solution (Laskar et al., 2004) Long-eccentricity: red line; short-eccentricity: blue line) and its 405-kyr sinusoidal filtered component (red line). (d) Tuned Spliced MS (black line) and 405-kyr component (red line) of ODP Site 1049 and its associated 405-kyr component (red line). The ages of rapid reversals within the CNPS resulting from the tuning are highlighted in green.

The cyclostratigraphic evaluation of the MS record from ODP Site 1049 supports the conclusion that sedimentation during the analyzed interval was modulated by orbital forcing, with a clear imprint of both long- and short-eccentricity cycles. Based on the age model derived from the tuning process, it was also possible to evaluate the SAR, to date the CORB intervals and to correlate them with those identified in the PLG core (Coccioni et al., 2012; Ramos et al., 2025) (~~Figure~~ Fig. 6).

In the Aptian, CORB A showed a strong correlation with CORB 1 from the PLG core (Coccioni et al., 2012). Both intervals, with durations exceeding 1 Myr, can be classified as long-term CORBs (Hu et al., 2012). Although there were smaller, darker

layers (short-term CORBs; Hu et al., 2012) within CORB A, with durations corresponding to Milankovitch cycles, almost all the Aptian sedimentation at ODP Site 1049 between 115.8 and 114.5 Ma consists of reddened sediments. In addition to the short-term CORBs, which reflect orbital forcing, there were other distinctly reddish intervals with durations of ~350 and ~210 kyr. These intervals have durations that do not correspond to any known orbital cycle (~~Figure~~ Fig. 6, left).

The basal section of the Albian stage, which was also affected by the unconformity (absence of the *Microhedbergella renilaevis* planktonic foraminifera Zone), is characterized by the absence of CORBs. The CORB 3, associated with the Monte Nerone level, is also absent.

Similarly to the PLG core, but with distinct durations, the ~400-kyr-long ~~lasting~~ interval following the first occurrence (FO) of the *H. albiensis* nannofossil Zone is composed of sediments predominantly green in color. The onset of the black shale, corresponding to the Urbino Level, is marked by a shift from yellow-greenish to black coloration. This event begins at 111.66 Ma and lasts for approximately 70 kyr (~~Figure~~ Fig. 6). CORB B starts at ~~115~~111.50 Ma in the ODP 1049 section and consists of at least eight main levels of reddish-brown coloration, with durations consistent with Milankovitch cycles. The high concentration of hematite in this interval (Hu et al., 2006a,b) results in a significantly larger MS amplitude compared to the rest of the studied section. After the termination of CORB B (~110.97 Ma), an interval with alternating yellowish and greenish hues predominates until the onset of CORB C at ~110.84 Ma. The onset of CORB C is gradual, allowing for a potential correlation with CORB 4. However, despite the possible correlation between the onsets of CORB C (ODP Site 1049) and CORB 4 (PLG core), the latter exhibits a shorter duration (~~Figure~~ Fig. 6).

The eight main CORB levels composing CORB B (Fig. 6) have the following thicknesses and estimated durations (from oldest to youngest): ~55 cm / 125 kyr; 12 cm / 39 kyr; 7 cm / 23 kyr; 34 cm / 95 kyr; 12 cm / 39 kyr; 5 cm / 18 kyr; 6 cm / 22 kyr; and 5 cm / 18 kyr. For CORB C, from oldest to youngest, the values are: ~12 cm / 39 kyr; 5 cm / 18 kyr; 5 cm / 18 kyr; 5 cm / 18 kyr; 5 cm / 18 kyr; 7 cm / 23 kyr; 12 cm / 39 kyr; 7 cm / 23 kyr; 34 cm / 95 kyr; and 12 cm / 39 kyr. It should be noted that these values are approximate, as some red beds appear (and disappear) abruptly, whereas others show more gradational boundaries.

The cyclic patterns are consistent with enhanced variability in bottom-water ventilation and primary productivity, in agreement with previous observations of orbitally paced changes in Early Cretaceous deep-ocean oxygenation (Herbet et al., 1986; Leandro et al., 2022; Gambacorta et al., 2016). In contrast, Aptian proxies display more uniform behavior, with low-amplitude $CaCO_3$ variations and the absence of clear productivity cycles (Fig. 3). This suggests a more stable paleoceanographic regime during the Aptian, likely maintained by restricted oceanic connectivity prior to the full opening of the Equatorial Atlantic Gateway (EAG; Duarte et al., 2025; Ramos et al., 2025) and by the persistence of the Cold Snap climatic state. Orbital pacing, however, is still recorded in Aptian MS fluctuations, indicating sensitivity to insolation forcing even under comparatively steady circulation.

Formatado: Cor da fonte: Automática

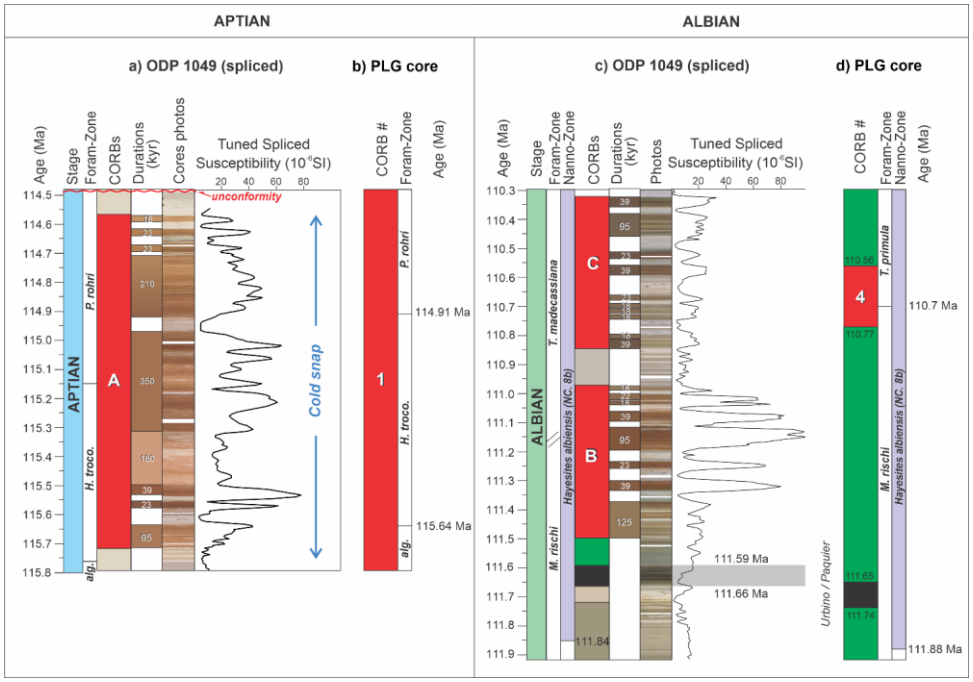

Figure 6: a) Aptian interval from ODP Site 1049, highlighting the time spans of the CORBs layers. b) Aptian interval from the PLG core. c) Albian interval from ODP Site 1049, illustrating the time spans corresponding to the CORBs layers and the Urbino/Paquier Level (indicated by the grey rectangle). d) Albian interval from the PLG core, depicting the durations associated with the CORBs and the Urbino Level (represented by the black rectangle). Age models and CORBs boundaries follow Ramos et al. (2024a) and Coccioni et al. (2012).

5 Discussions

5.1 Aptian–Albian paleoclimatic reorganization of ocean circulation ~~1 Diachronism between the Tethys and North Atlantic Oceans~~

A major paleoclimatic transition across the Aptian–Albian boundary is recorded by long-term fluctuations in the carbon isotope record, reflecting changes in the global carbon cycle linked to ocean circulation and productivity (Weissert, 1989). At ODP Site 1049, $\delta^{13}C$ values shift abruptly from ~4‰ to ~2‰ VPDB, providing clear evidence for a fundamental climatic reorganization (Huber et al., 2011). Independent proxies, including floral and faunal turnover, plant fossils indicating cooler conditions, glendonites, ice-rafted debris, and intensified hydrological cycling associated with the late Aptian Equatorial Humid Belt, corroborate this transition (Hochuli, 1981; Krassilov, 1973; Leckie, 1989; Kemper, 1987; Herrle et al., 2015; Santos et al., 2022; Ramos et al., 2025). Tethyan records further indicate reduced siliciclastic input, turnover within the *G. algerianus* Zone, and a pronounced global sea-level fall (Weissert and Lini, 1991).

This cooling, often termed the Aptian "Cold Snap" (McAnena et al., 2013), is commonly attributed to declining atmospheric CO_2 levels, likely driven by enhanced burial of organic carbon and pyrite, which slowed carbon cycling and promoted polar ice growth (Weissert and Lini, 1991; Leandro et al., 2022). Large Igneous Province (LIP) emplacement, particularly the Kerguelen Plateau, may have contributed to this climate shift by perturbing the carbon cycle and triggering episodic cooling (Coffin and Eldholm, 1994; Percival et al., 2024). Geochemical proxies, including benthic and planktonic $\delta^{18}O$, indicate that Aptian bottom waters were up to ~10°C cooler than those of the Albian, highlighting a rapid warming of both surface and deep waters across the boundary (Huber et al., 2011; Kochhann et al., 2023).

Under typical Cretaceous greenhouse conditions, high-latitude regions were unlikely to generate dense, oxygenated deep waters, leading to sluggish deep-ocean ventilation (Schlanger and Jenkyns, 1976; Hay, 2008, 2009). The Aptian Cold Snap temporarily disrupted this mode, enhancing thermohaline circulation through increased oxygen solubility in colder waters and possibly the presence of polar ice. This circulation regime promoted deep-water renewal and organic matter oxidation, processes that facilitated CORB formation, as evidenced by widespread hardgrounds, intensified bottom currents, and a basin-wide shift from grey-green to red-brown sediments (Premoli Silva et al., 1989; Weissert and Lini, 1991).

During the Albian, renewed greenhouse conditions suppressed deep-water formation by reducing latitudinal thermal gradients, with ocean heat transport dominated by mesoscale eddies and low-latitude sinking of warm, saline waters (Hay, 2008, 2009; Gambacorta et al., 2016). This shift is reflected in clay-mineral assemblages and geochemical proxies: Aptian Ca-rich CORBs formed under drier conditions with limited terrigenous input, whereas Albian Al-rich CORBs indicate more humid climates, greater paleoceanographic variability, and orbitally paced alternations in ventilation (Li et al., 2011; Hu et al., 2012).

The slightly higher illite concentrations in the Aptian CORBs—reflecting moderate to weak weathering under relatively dry conditions—suggest that the atypical conditions of the Aptian Cold Snap interlude were characterized by lower terrigenous input than that experienced during the Albian (Fig. 3). Although the $CaCO_3$ content of the white layers interbedded with the red beds is similar in the Aptian and Albian intervals, the markedly low $CaCO_3$ values in the Albian CORBs are noteworthy

Formatado: Inglês (Estados Unidos)
Formatado: Inglês (Estados Unidos)
Formatado: Fonte: Itálico, Inglês (Estados Unidos)
Formatado: Inglês (Estados Unidos)
Formatado: Inglês (Estados Unidos)
Formatado: Inglês (Estados Unidos)
Formatado: Inglês (Estados Unidos)
Formatado: Inglês (Estados Unidos)
Formatado: Inglês (Estados Unidos)
Formatado: Cor da fonte: Texto 1

(Li et al., 2011). This observation indicates substantial paleoceanographic variability (instability) during the Albian compared to the Aptian stage. Low $CaCO_3$ content may be related to: (a) reduced primary productivity, (b) higher dissolved CO_2 concentrations, (c) increased terrigenous input, and (d) water-column stagnation with the absence of younger waters. Because terrigenous input at ODP Site 1049 remained stable throughout the Albian (Cheng, 2008), we propose that alternation between intervals of active water bottom oxygenation and intervals of ocean stagnation (white and green beds) provides a more plausible explanation. Variations in the Ba/Al ratio and in SiO_2 and Al_2O_3 concentrations between the Albian red and white beds (Fig. 3) further support the presence of cyclical changes in productivity (Hu et al., 2012). In contrast, the absence of such abrupt $CaCO_3$ variability during the Aptian suggests more stable paleoceanographic conditions, with limited fluctuations in paleoproductivity and ocean circulation.

5.2 Circulation regimes and CORB formation

CORBs serve as key archives of mid-Cretaceous climate and circulation dynamics (Premoli Silva et al., 1989; Hu et al., 2005; Li et al., 2011; Giorgioni et al., 2017; Gambacorta et al., 2016). Their formation is linked to episodes of cold, oxygenated deep-water formation rather than elevated productivity, as LIP-derived nutrients would have promoted organic carbon burial incompatible with oxidized conditions (Leckie et al., 2002; Browning and Watkins, 2008; Wang et al., 2009). Enhanced burial of organic carbon during OAEs, combined with LIP-induced perturbations, reduced atmospheric CO_2 and promoted global cooling, increasing the oxidizing capacity of deep waters during the Aptian Cold Snap (Arthur et al., 1988; Weissert, 1989; Hu et al., 2012).

Aptian CORBs are long-lived, regionally correlatable, and reflect sustained thermohaline circulation over ~2 Myr, supported by isotopic evidence for well-oxygenated, cooler, and low-productivity deep waters (Erbacher et al., 2001; Premoli Silva et al., 1989; Leandro et al., 2022). Enhanced vertical mixing driven by current–topography interactions may have further facilitated oxygenation (Ahmerkamp et al., 2017).

In contrast, Albian CORBs are shorter, orbitally paced, and reflect transient ventilation interspersed with stratification and episodic black shale deposition (Paquier/Urbino Level; Erbacher et al., 2001). Color, facies, and geochemical variability among Albian CORBs indicate localized differences in paleogeography and oceanography, with obliquity and short-eccentricity cycles controlling sedimentation (Li et al., 2011; Trabucho Alexandre et al., 2011). Aptian CORBs display more uniformity, consistent with sustained circulation and restricted oceanic connectivity prior to full opening of the Equatorial Atlantic Gateway (Dummann et al., 2023; Ramos et al., 2025).

One of the most frequently mentioned characteristics of CORB deposition is its association with low sedimentation rates in pelagic deep waters of oceanic basins (Wang et al., 2009; Hu et al., 2012). Previous studies have estimated sedimentation rates in the Aptian section of ODP Hole 1049C to range between 0.25 and 0.35 cm/kyr, based on the *Paraticinella eubejaouaensis* (*Paraticinella* rohri) and *Globigerinelloides algerianus* zones (Li et al., 2011). Additional estimates using paleomagnetic data and astronomical tuning have inferred sedimentation rates of 0.4 cm/kyr during the late Aptian and up to 1 cm/kyr in the early

Formatado: Cor da fonte: Texto 1
Formatado: Inglês (Reino Unido)
Formatado: Inglês (Estados Unidos)
Formatado: Inglês (Estados Unidos)
Formatado: Inglês (Estados Unidos)
Formatado: Inglês (Estados Unidos)
Formatado: Inglês (Estados Unidos)

Albian (Ogg and Bardot, 2001; Ogg et al., 1999). In contrast, our study provides sedimentation rates ranging from 0.5 to 0.9 cm/kyr for the Aptian section and from 0.6 to 0.8 cm/kyr for the Albian section at ODP Site 1049 (Fig. 5). Notably, these values do not indicate significant variations that would support the hypothesis of extremely slow sediment accumulation as a primary control on CORB formation, as previously proposed (Wang et al., 2009).

5.3 Geological synchrony between the Tethyan and North Atlantic oceans

Formatado: Título 1

~~One of the most notable characteristics of CORBs deposition is their association with low sedimentation rates at pelagic, deep water in oceanic basins (Wang et al., 2009; Hu et al., 2012). Previous studies have estimated sedimentation rates in the Aptian section of ODP Hole 1049C to range between 0.25 and 0.35 cm/kyr, based on the *Paraticinella eubejaouaensis* and *Globigerinelloides algerianus* zones (Li et al., 2011). Additional estimates using paleomagnetic data and astronomical tuning have inferred sedimentation rates of 0.4 cm/kyr during the late Aptian and up to 1 cm/kyr in the early Albian (Ogg and Bardot, 2001; Ogg et al., 1999). In contrast, our study provides sedimentation rates ranging from 0.5 to 0.9 cm/kyr for the Aptian section and from 0.6 to 0.8 cm/kyr for the Albian section at ODP Site 1049 (Figure 5). Notably, these values do not indicate significant variations that would support the hypothesis of extremely slow sediment accumulation as a primary control on CORB formation, as previously proposed (Wang et al., 2009).~~

Correlations between CORBs at ODP Site 1049 and those identified in the PLG core provide insight into the temporal synchrony of these deposits and the paleoceanographic conditions under which they formed. Using first occurrences (FO~~s~~) of key planktonic foraminiferal biozones—recognized as more reliable markers for diachronism studies (Berggren and Van Couvering, 1974)—our analysis shows that the *H. trocoidea* zone spans 0.73 Myr in the Tethys (115.64 to 114.91 Ma, PLG core; Ramos et al., 2025), while its duration in the North Atlantic is slightly shorter, at 0.61 Myr (115.75 to 115.14 Ma, ODP Site 1049; this study).

~~For the OAE 1b-related black shale in ODP Hole 1049C, Erbacher et al. (2001) estimated a duration of approximately 46 kyr. Our results, however, indicate a slightly longer duration of 70 kyr and a central age of 111.63 Ma. This interval correlates with the Urbino Level (111.74 to 111.65 Ma; Figure 6). Given the small age and duration differences, this event can be considered effectively synchronous between the Tethyan and North Atlantic domains.~~ The FO of the nannofossil *H. albiensis* marks the base of the NC8B subzone (Bralower et al., 1993~~, 1995~~) and shows a temporal offset of only 40 kyr between basins (Huber et al., 2011; Ramos et al., 2025).

For the OAE 1b-related black shale in ODP Hole 1049C, Erbacher et al. (2001) estimated a duration of approximately 46 kyr. Our results, however, indicate a slightly longer duration of 70 kyr and a central age of 111.63 Ma. This interval correlates with the Urbino Level (111.74 to 111.65 Ma; Fig. 6). Even with marked differences in oxidation levels observed through the correlation (in geological time) between the Albian interval of ODP Site 1049 and the PLG core—differences dependent on palaeogeographic and depositional settings (Trabucho Alexandre et al., 2011)—the small age and duration offsets indicate that

this event can be considered effectively synchronous between the Tethyan and North Atlantic domains. This observation suggests that the widespread anoxia associated with this particular OAE 1b sub-event transcends local physiographic barriers, supporting its interpretation as a truly global phenomenon.

The astrochronological tuning applied in this study yields a maximum error of ~200 kyr (half of the long-eccentricity cycle period of 405 kyr used in the tuning) over a 250 Myr timespan, or roughly ~1.6‰ (Laskar, 2020). Both the ~100 kyr difference in the duration of the *H. trocoidea* zone and the discrepancies in FO and LO ages fall within this error range, preventing a conclusive assessment of dispersal mechanisms (Petrizzo, 2003; Lam et al., 2022). However, the strong synchrony observed for both the Urbino Level and the FO of *H. albiensis* across the two oceanic regions was expected due to the relatively short distance between the North Atlantic and the Tethyan Ocean, which, together with the presence of persistent easterly equatorial winds (Hay, 2008), favored rapid dispersal.

~~The astrochronological tuning applied in this study yields an error margin of approximately 405 kyr over a 250 Myr timespan, or roughly ~1.6‰ (Laskar, 2020). Both the ~100 kyr difference in the duration of the *H. trocoidea* zone and the discrepancies in FO and LO ages fall within this error range, preventing a conclusive assessment of dispersal mechanisms (Petrizzo, 2003; Lam et al., 2022). However, the strong synchrony observed for both the Urbino Level and the FO of *H. albiensis* across the two oceanic regions suggests a north-to-south migration pattern of *H. trocoidea* from the North Atlantic into the Tethyan Ocean.~~

5.~~2~~4 ~~Synchronism and origin of~~ Milankovitch-band orbital forcing of CORB deposition ~~CORBs~~

High-frequency Milankovitch-scale cyclicity is widely recorded in Lower Cretaceous pelagic successions and is expressed in variations of $CaCO_3$ and SiO_2 contents (Herbert et al., 1986), carbon isotopes, and magnetic susceptibility (Leandro et al., 2022). These cycles are superimposed on a long-term perturbation of the global carbon cycle (Weissert, 1989), characterized by reduced carbon turnover and multi-million-year cold interludes (Leandro et al., 2022), potentially associated with polar ice-sheet growth (Trabucho Alexandre et al., 2011) and eustatic sea-level fall (Weissert and Lini, 1991).

Orbital-scale variability in ocean circulation reflects the interplay between seasonal contrast, hydrological balance, and water-column stratification. Humid climates with strong seasonality favor stratification and are typically associated with non-CORB intervals, whereas reduced seasonality under more arid conditions promotes weaker stratification and CORB deposition (Giorgioni et al., 2017). Variations in runoff, evaporation, saline exchange between basins, and temperature-dependent oxygen solubility further modulate surface-water density gradients and deep-water formation (Ryan and Cita, 1977; Weissert et al., 1985; MacLeod et al., 2001; Steinig et al., 2024). Episodic saline incursions and astronomically paced bottom currents may have intermittently enhanced deep-water renewal and seafloor reoxygenation without requiring major reorganization of global circulation (Friedrich et al., 2008; Gambacorta et al., 2016).

Formatado: Inglês (Estados Unidos)
Formatado: Inglês (Estados Unidos)
Formatado: Inglês (Estados Unidos)
Formatado: Inglês (Estados Unidos)
Formatado: Inglês (Estados Unidos)
Formatado: Inglês (Estados Unidos)

At ODP Site 1049, the Albian interval displays pronounced orbital-scale cyclicity in $CaCO_3$, Ba/Al, SiO_2, Al_2O_3, and magnetic susceptibility (Li et al., 2021; Hu et al., 2022), consistent with repeated alternations between enhanced ventilation and stratified conditions (Figs. 3 and 4). Albian CORBs are best explained by the combined effects of evaporation-driven deep-water formation—through episodic saline flooding—and orbitally regulated bottom-current activity that transiently reoxygenated the seafloor, enabling cyclic early diagenesis. In contrast, the Aptian interval shows more uniform proxy behavior, limited $CaCO_3$ variability, and weaker productivity signals, pointing to a comparatively stable circulation regime. Although orbital forcing is still expressed in magnetic susceptibility, its impact was muted, consistent with sustained deep-water ventilation during the Aptian cold snap and restricted oceanic connectivity prior to the full opening of the Equatorial Atlantic Gateway.

~~The relationship between the origin of CORBs and episodes of cold deep-water formation (Hu et al., 2005; Li et al., 2011) is one of the most compelling aspects of their paleoenvironmental significance, as it positions these red layers as critical paleoclimatic archives. Early hypotheses suggested that black shales served as sources of ferrous iron, which diffused upward into slowly accumulating oxygenated clays, promoting hematite formation (Arthur, 1979). However, large intervals of CORBs—such as the Aptian section at ODP Site 1049—are not associated with any underlying black shales, challenging this model.~~

~~The onset of widespread CORB deposition following the OAE 1a (Wang et al., 2009) supports a potential link with the emplacement of LIPs, including the Southern Kerguelen Plateau, Nauru–Mariana Plateau, and Ontong Java Plateau (Eldholm and Coffin, 2000; Matsumoto et al., 2021, 2022; Percival et al., 2024). Micronutrients released during these LIP events may have stimulated surface ocean productivity (Browning and Watkins, 2008; Leckie et al., 2002), initiating brief productivity pulses prior to CORB 1 in the PLG core (Coccioni et al., 2012; Sabatino et al., 2018) and CORB A at ODP Site 1049 (this study). However, the elevated productivity and increased organic matter flux associated with these pulses are inconsistent with the high-oxygen-demand conditions required for CORB formation (MacLeod et al., 2001; Wang et al., 2009; Hu et al., 2012). More plausibly, the emplacement of LIPs contributed to the initiation of the Aptian "Cold Snap" period (McAnena et al., 2013), a significant cooling episode that altered ocean circulation patterns. Wang et al. (2011) proposed that CORBs may represent a consequence of global climatic cooling and deep-ocean ventilation following OAEs. Enhanced organic carbon and pyrite burial during OAEs would have reduced atmospheric pCO_2, triggering global cooling and increasing the oxidizing potential of deep waters (Hu et al., 2012; Arthur et al., 1988). This model provides a partial explanation for the origin of long-term CORBs.~~

~~The global reach and persistence of cold, oxygenated bottom waters during the Cold Snap are supported by the observed synchrony between CORB 1 (Tethys) and CORB A (North Atlantic) (Figure 4). Although internally modulated by orbital-scale forcing (Hu et al., 2012), the absence of greenish sediment layers throughout much of the late Aptian further supports the hypothesis of globally pervasive oxic conditions. Thus, the most likely mechanism behind the formation of the Aptian long-term CORBs is a sustained and effective thermohaline circulation, intensified during the prolonged (~2 Myr) Cold Snap (Hu et al., 2012; McAnena et al., 2013; Leandro et al., 2022). Vertical mixing driven by current-topography interactions (e.g.,~~

Formatado: Inglês (Estados Unidos)

Formatado: Normal

seamounts, ridges) may also have transported oxygen to deeper waters, enhancing bottom-water ventilation (Ahmerkamp et al., 2017). Isotopic evidence from ODP Site 1049 supports this interpretation. Data from the upper Aptian interval show a well-mixed, ventilated water column, characterized by cold temperatures and low productivity (Erbacher et al., 2001). These conditions were followed by slightly warmer, less saline surface waters that promoted water column stratification and the deposition of a black shale horizon, identified in this study as the Urbino Level. In contrast, the Albian interval marks a return to ventilated, oxygenated conditions, indicative of a breakdown in ocean stagnation (Figure 6).

Compared to Aptian, the Albian CORBs are shorter in duration, suggesting more heterogeneous paleoceanographic conditions. Based on sediment thickness and accumulation rates, Li et al. (2011) estimated the duration of Albian CORB cycles to correspond to Milankovitch-band periodicities, specifically obliquity (~53.6 kyr) and short eccentricity (85–140 kyr). Our study confirms that the durations of the reddish/brown layers align well with these orbital cycles (Waltham, 2015; Laskar, 2020), suggesting a strong orbital control over Albian CORB deposition.

Additionally, transient climate events—such as cyclones, intense storms, and forced upwelling—may have intermittently oxygenated bottom waters through enhanced vertical mixing (Rovelli et al., 2016). Variations in continental runoff and precipitation could have also modulated deep-water convection and oxygenation (Bice et al., 1997). These mechanisms are thought to have triggered some of the Albian OAEs, including the black shale at ODP Site 1049, interpreted here as the Urbino Level (Erbacher et al., 2001; Matsumoto et al., 2022). However, the expression of the Urbino Level in the Umbria-Marche Basin appears to be unrelated to continental detrital input—indicated by low Fe and Ti content—and is instead linked to a major transgressive event (Ramos et al., 2024b).

In summary, while both Aptian and Albian CORBs reflect the influence of multiple climate drivers, their duration and geographic extent differ significantly. The Aptian long-term CORBs were likely shaped by sustained thermohaline circulation and global cooling during the Cold Snap, whereas the Albian CORBs were more sensitive to orbital forcing and regional climatic variability, resulting in shorter, cyclic red bed intervals.In summary, while both Aptian and Albian CORBs reflect the influence of multiple climate drivers, their duration and geographic extent differ significantly. The Aptian long-term CORBs were likely shaped by sustained thermohaline circulation and global cooling during the Cold Snap, whereas the Albian CORBs were more sensitive to orbital forcing and regional climatic variability, resulting in shorter, cyclic red bed intervals.

5.3 5 Long-cycle-related unconformity

Climatic precession is modulated by short eccentricity, which in turn is controlled by long eccentricity (Laskar et al., 2004). The 2.4-Myr longer-period cycle (defined by g_4-g_3, related to the precession of the perihelion) not only modulate the 405-kyr eccentricity (Olsen et al., 2019) but has been also reported as exerting significant influence on climate (Kocken et al., 2019; Boulila, 2019) and ocean circulation patterns (Dutkiewicz et al., 2024).

~~Incomplete stratigraphic records near the Aptian–Albian boundary (associated with the OAE 1b event; Ramos et al., 2024b) are not uncommon. In addition to ODP Site 1049, other drill sites, such as DSDP Sites 390, 392A, and 511 (among others), also show the absence of upper Aptian and lower Albian sections (see Huber et al., 2011). Dutkiewicz et al. (2024) presented a comprehensive synthesis of data from scientific deep-sea drilling sites, suggesting that these observed hiatus cycles are linked to orbitally driven increases in deep-water circulation intensity and enhanced erosive activity by bottom currents.~~

~~This depositional gap has led to discrepancies in the characterization of the amplitude and duration of OAE 1b (Ramos et al., 2024b). Efforts to correlate OAE 1b on a global scale using carbon isotope excursions and the nomenclature of organic-rich levels (or OAE 1b sub-events) have resulted in misunderstandings regarding its significance and extent (e.g., Herrle et al., 2004, 2010, 2015; Trabucho-Alexandre et al., 2011; Kennedy et al., 2014; Coccioni et al., 2014). In the Vocontian Basin, four organic-rich levels—Jacob, Kilian, Paquier, and Leenhardt (Bréhéret, 1994)—have been considered representative of OAE 1b, although some studies recognize only Jacob, Kilian, and Paquier (Trabucho-Alexandre et al., 2011), or just Paquier (Herrle et al., 2004). The expression of OAE 1b in complete Tethyan Ocean sections (Coccioni et al., 2012, 2014) cannot be directly correlated with the incomplete records of the North (ODP Site 1049; Huber and Leckie, 2011) and South (DSDP Site 511) Atlantic regions.~~

The unconformity observed at ODP Site 1049 is consistent with the local geological setting of the Blake Escarpment, a continental-slope environment characterized by persistent bottom-current activity and high erosional potential (Benson et al., 1978; Li et al., 2011). Along continental margins in both the Tethyan Ocean and the North Atlantic, buried contourite drifts and stratigraphic gaps are common features and are widely attributed to variations in bottom-current strength and reorganizations of deep-water circulation, frequently linked to OAEs and major paleoceanographic transitions (Gambacorta et al., 2016; Liu et al., 2023).

However, hiatuses of comparable duration have been documented at multiple sites, including DSDP Sites 511, 545, 763B, and 392A (Huber and Leckie, 2011), as well as at DSDP Site 545 off Morocco and ODP Site 1276 in the Newfoundland Basin (Trabucho Alexandre et al., 2011). The recurrence of similarly timed unconformities across different ocean basins indicates that the discontinuity at Site 1049 reflects a regional to global paleoceanographic signal rather than a purely local phenomenon. Incomplete stratigraphic records near the Aptian–Albian boundary—commonly associated with OAE 1b (Ramos et al., 2024b)—are therefore not unusual; several drill sites, including DSDP Sites 390, 392A, and 511, show partial or complete removal of upper Aptian and lower Albian successions (Huber et al., 2011).

Independent support for an erosional surface at ODP Site 1049 is provided by abrupt shifts in $\delta^{18}O$, $\delta^{13}C$, and $^{87}Sr/^{86}Sr$ ratios, coincident with the major planktic foraminiferal extinction at the Aptian–Albian boundary and expressed lithologically as a sharp contact. In addition, the $CaCO_3$ record shows a pronounced decrease indicative of dissolution and/or sediment removal (Li et al., 2011), further supporting the presence of a depositional hiatus. While initial estimates placed the duration of this gap at ~0.8–1.4 Myr (Huber et al., 2011), astrochronological constraints indicate that the absence of the *Microhedbergella renilaevis* and *M. miniglobularis* zones corresponds to ~0.76–0.84 Myr (Ramos et al., 2024). Because the overlying *M. rischi* zone may also be incomplete at Site 1049, the total duration of the unconformity likely exceeded 2 Myr.

Formatado: Inglês (Estados Unidos)

Formatado: Inglês (Estados Unidos)

Formatado: Inglês (Estados Unidos)

Formatado: Inglês (Estados Unidos)

This extended depositional gap has contributed to discrepancies in the estimated amplitude and duration of OAE 1b (Ramos et al., 2024b) and complicates global correlations based on carbon-isotope excursions or the nomenclature of organic-rich sub-events. In the Vocontian Basin, up to four organic-rich horizons—Jacob, Kilian, Paquier, and Leenhardt (Bréhéret, 1994)—have been attributed to OAE 1b, whereas other studies recognize fewer levels (Herrle et al., 2004; Trabucho Alexandre et al., 2011). Consequently, the expression of OAE 1b in complete Tethyan sections (Coccioni et al., 2012, 2014) cannot be straightforwardly correlated with the incomplete records of the North and South Atlantic basins, including ODP Site 1049 and DSDP Site 511.

Multiple processes likely contributed to the development of the Aptian–Albian unconformity. Paleoclimatic reconstructions indicate cooler temperatures and reduced humidity during this transition, coincident with high-latitude cooling and a global sea-level fall, consistent with the buildup of polar ice caps (Weissert and Lini, 1991). Carbon-cycle perturbations during the Aptian closely track eustatic variations (Haq et al., 1987), and the pronounced negative $\delta^{13}C$ excursion at the base of the Albian (C-mark v; Ramos et al., 2024) coincides with a lowstand. We therefore propose that eustatic sea-level fall was a primary control on sediment removal at ODP Site 1049, while bottom-current activity acted as an amplifying mechanism rather than the initial driver of erosion.

Although the progressive opening of the Equatorial Atlantic Gateway during the Albian may have strengthened contour currents along continental slopes (Duarte et al., 2025), the presence of a comparable unconformity at DSDP Site 511 in the southern South Atlantic suggests that intensified bottom currents were a response to global sea-level change rather than a purely gateway-driven process. Transient bottom currents, potentially modulated by orbital forcing, may have further promoted episodic seafloor erosion and reoxygenation (Gambacorta et al., 2016). The estimated duration of ~2.56 Myr for the unconformity at ODP Site 1049 is compatible with long-period (~2.4 Myr) eccentricity modulation, supporting recent suggestions that grand orbital cycles exerted a first-order control on global deep-water circulation and sediment preservation prior to 70 Ma (Dutkiewicz et al., 2024).

Overall, the long duration and widespread expression of the Aptian–Albian unconformity likely reflect the superposition of eustatic, climatic, and circulation-driven processes operating under distinct mid-Cretaceous boundary conditions.

~~Interestingly, our findings indicate a timespan of ~2.56 Myr associated with the unconformity at ODP Site 1049 (Figures 5c and 5d), which is also compatible with a recent suggestion (e.g., Dutkiewicz et al., 2024) that ~2.4-Myr grand cycles may have caused global hiatuses prior to 70 Ma. Correlations of deep-water records spanning the interval from approximately 114.5 to 111.9 Ma may be biased due to this erosive event.~~Incomplete stratigraphic records near the Aptian–Albian boundary ~~(associated with the OAE 1b event; Ramos et al., 2024b) are not uncommon. In addition to ODP Site 1049, other drill sites, such as DSDP Sites 390, 392A, and 511 (among others), also show the absence of upper Aptian and lower Albian sections (see Huber et al., 2011). Dutkiewicz et al. (2024) presented a comprehensive synthesis of data from scientific deep-sea drilling sites, suggesting that these observed hiatus cycles are linked to orbitally driven increases in deep-water circulation intensity and enhanced erosive activity by bottom currents.~~

Formatado: Inglês (Estados Unidos)

Formatado: Inglês (Estados Unidos)

~~This depositional gap has led to discrepancies in the characterization of the amplitude and duration of OAE 1b (Ramos et al., 2024b). Efforts to correlate OAE 1b on a global scale using carbon isotope excursions and the nomenclature of organic-rich levels (or OAE 1b sub-events) have resulted in misunderstandings regarding its significance and extent (e.g., Herrle et al., 2004, 2010, 2015; Trabucho-Alexandre et al., 2011; Kennedy et al., 2014; Coccioni et al., 2014). In the Vocontian Basin, four organic-rich levels—Jacob, Kilian, Paquier, and Leenhardt (Bréhéret, 1994)—have been considered representative of OAE 1b, although some studies recognize only Jacob, Kilian, and Paquier (Trabucho-Alexandre et al., 2011), or just Paquier (Herrle et al., 2004). The expression of OAE 1b in complete Tethyan Ocean sections (Coccioni et al., 2012, 2014) cannot be directly correlated with the incomplete records of the North (ODP Site 1049; Huber and Leckie, 2011) and South (DSDP Site 511) Atlantic regions.~~

~~Interestingly, our findings indicate a timespan of ~2.56 Myr associated with the unconformity at ODP Site 1049 (Figures 5c and 5d), which is also compatible with a recent suggestion (e.g., Dutkiewicz et al., 2024) that ~2.4 Myr grand cycles may have caused global hiatuses prior to 70 Ma. Correlations of deep-water records spanning the interval from approximately 114.5 to 111.9 Ma may be biased due to this erosive event.~~

~~Climatic precession is modulated by short eccentricity, which in turn is controlled by long eccentricity (Laskar et al., 2004). The 2.4 Myr longer-period cycle (defined by g_4–g_3, related to the precession of the perihelion) not only modulate the 405-kyr eccentricity (Olsen et al., 2019) but has been also reported as exerting significant influence on climate (Kocken et al., 2019; Boulila, 2019) and ocean circulation patterns (Dutkiewicz et al., 2024).~~

5.~~4~~ 6 Short geomagnetic reversed-polarity subchrons

Since Ryan et al. (1978) introduced a nomenclature from M-1r to M-3r for the series of brief reversed-polarity subchrons within the Aptian–Albian, geomagnetic reversals during the CNPS have been reported and dated worldwide (Shi et al., 2004; Tarduno, 1990; Zhang et al., 2021; Ramos et al., 2024b). The M0r Chron (120.29 to 119.70 Ma; Li et al., 2023) marks the base of the Aptian and the CNPS (Savian et al., 2016; Leandro et al., 2022). This reverse chron is a proposed marker for the Barremian–Aptian boundary (Helsley and Steiner, 1968; Gale et al., 2020; Zhang et al., 2021), and its age and duration are crucial factors for constraining past oceanic, tectonic, and geodynamic behavior (Li et al., 2023). The base of this chron is dated at ~120.2 Ma by astrochronology (Leandro et al., 2022) and 120.29 ± 0.09 Ma by integration of U–Pb and $^{40}Ar/^{39}Ar$ ages (Li et al., 2023). The M-1r reversal, or ISEA (VandenBerg et al., 1978), represents the first Aptian short geomagnetic reversed-polarity subchron after the M0r Chron. Positioned within the planktonic foraminiferal zone of *G. algerianus* (Tarduno, 1990; Ramos et al., 2024a), this reversal has an estimated age of 117.03 ± 0.14 Ma, with a timespan of approximately 20 kyr. The

next reversal event, referred to as "2" (Ramos et al., 2024a), has an estimated age of 116.17 ± 0.14 Ma and a timespan of approximately 10 kyr.

The first pair of reversals above the M0r Chron is within the upper Aptian (Ryan et al., 1978; Zhang et al., 2021; Ramos et al., 2024b). Approximately 5 Myr younger, another pair of reversals is observed within the CNPS (Ryan et al., 1978). Despite the absolute dating range via $^{40}Ar/^{39}Ar$ of basalt flows dated at 113.3 ± 1.6 Ma from the Tuoyun section (China), which suggests an additional reversal in the upper Aptian (Gilder et al., 2003), our study indicates that this reversal occurred during the lower Albian (~~Figure~~ Fig. 7), as proposed by Ryan et al. (1978). The stratigraphically youngest reversal of the second pair, referred to here as "3," spans between 111.45 and 111.53 Ma. Due to the low temporal resolution of the paleomagnetic data obtained by Ogg and Bardot (2001), the timespan of ~ 80 kyr may be overestimated.

The short reversed-polarity subchron "3" corresponds to reversal number 6 described by Zhang et al. (2021) and is located within the *M. rischi* planktonic foraminiferal Zone and near the FO of the *H. albiensis* calcareous nannofossil Zone (~~Figure~~ Fig. 5). These biostratigraphic markers may be useful in future studies. Although the possibility that this reversal represents a recording artifact cannot be entirely excluded, the exceptional preservation of both planktonic and benthic foraminifera—characterized by glassy shells and the absence of infilling calcite—strongly supports its authenticity (Erbacher et al., ~~2011~~2001). Additionally, the lack of homogenization in stable isotopic ratios further indicates that diagenetic overprinting is unlikely (Erbacher et al., ~~2011~~2001). Future high-resolution paleomagnetic investigations, in conjunction with cyclostratigraphic analyses, are expected to provide a more precise constraint on the duration of this reversal. Notably, a sample showing normal polarity (20X-2, 30–32~~, 202–30 cm~~) is located between the debated reversed-polarity sample and the overlying organic-rich black shale. This intervening sample displays even more pronounced yellowish to greenish staining in the original sediment, suggesting the preservation of its primary magnetization signal.

The M-2r reversal was initially identified in the 1970s as two distinct reversed events within the lower Albian, corresponding to the *Biticinella breggiensis* planktonic foraminiferal Zone of and the calcareous nannofossil zone of *Prediscosphaera cretacea* (Ryan et al., 1978). Later, in the Contessa valley section (Italy), Tarduno et al. (1992) described this interval as a complex and composite zone comprising two longer-lasting reversals (VC-R3 and VC-R7), accompanied by five shorter and less prominent reversed events (VC-R1, 2, 4, 5, and 6). Although there is a possibility that the reversed magnetizations could have resulted from intense seafloor oxidation processes (Tarduno et al., 1992), the M-2r event has also been recorded in association with the *B. breggiensis* and *P. cretacea* biozones.

The M-2r reversal set is also present in the Vientiane Basin (Ban Phonngam section; Zhang et al., 2021) as a pair of reversals at an approximate depth of 550 m, described as R4 and R5 (Zhang et al., 2021). Our study indicates that M-2r begins at 110.76 Ma, with a timespan of 150 kyr. Although this reverse event may be more complex (Tarduno et al., 1992), the available paleomagnetic data from ODP Site 1049 allow us to only infer a central age for this event. Similar to the interval observed between the ISEA and reversal "2" (Ramos et al., 2024a), our study shows that reversals "3" and M-2r are separated by ~800 kyr, supporting their interpretation as two distinct subchrons (~~Figure~~ Fig. 7). The cyclostratigraphic analysis performed in this

study enables the correlation of reversal "3" with the age of the reversal proposed through $^{40}Ar/^{39}Ar$ dating of basalt flows at 113.3 ± 1.6 Ma from the Tuoyun section (Gilder et al., 2003), making it an important tie point for future studies.

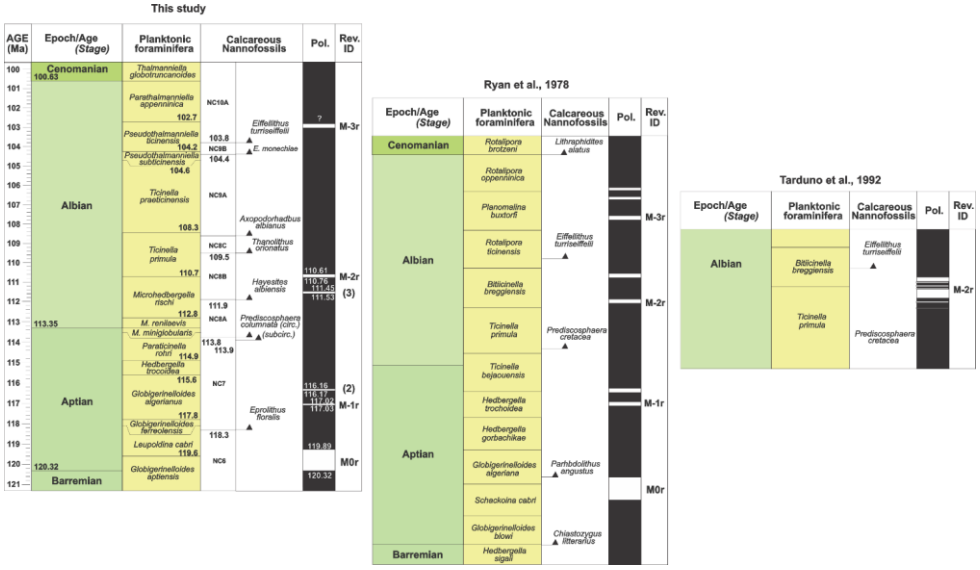

Figure 7: (Left) The stratigraphic framework with age (Ma) from the Aptian to the Cenomanian (this study), showing the ages of planktonic foraminiferal and calcareous nannofossil bioevents together with the geomagnetic polarity time scale (Pol.), including magnetic polarity reversals between 121 and 100 Ma and their corresponding reversal identifiers (Rev. ID). Ages are modified from GTS2020 and are consistent with the most recent age constraints of Leandro et al. (2022), Li et al. (2023, 2024), and Ramos et al. (2024a, 2024b). (Center) The stratigraphic framework with age showing the sets of reversals occurring during the Cretaceous Normal Superchron (CNPS) as originally proposed by Ryan et al. (1978). At that time, the first pair of reversals (M-1r) following the onset of the CNPS, defined by the M0r reversal, was correlated with the *Hedbergella trochoidea* bioevent. The second pair (M-2r), of Albian age, was correlated with the bioevents *Bitticinella breggiensis* and *Prediscosphaera cretacea*, and the third set of reversals with the bioevents *Planomalina buxtorfi* and *Eiffellithus turriseiffeli*. (Right) The stratigraphic framework proposed for Tarduno et al. (1992), updating definition of the reversal set that characterizes M-3r (Tarduno et al., 1992), occurring within the

Formatado: Inglês (Estados Unidos)
Formatado: Inglês (Estados Unidos)
Formatado: Inglês (Estados Unidos)
Formatado: Inglês (Estados Unidos)
Formatado: Inglês (Estados Unidos)
Formatado: Inglês (Estados Unidos)
Formatado: Inglês (Estados Unidos)
Formatado: Inglês (Estados Unidos)

Ticinella primula / *Bitticinella breggiensis* and *Prediscosphaera cretacea* biozones. Note the close proximity of this reversal set to the first occurrence (FO) of the *Eiffellithus turriseiffeli* zone.

~~(a) Modified Aptian–Albian timescale (b) Simplified timescale showing magnetic polarity ages (this study). (c) Geomagnetic polarity and reversal identification. (d) $^{40}Ar/^{39}Ar$ ages from Tuoyun Section (Gilder et al., 2003). (e) $^{40}Ar/^{39}Ar$ ages from Raajmahal Traps (Baksi, 1995). (f) $^{40}Ar/^{39}Ar$ ages from Sanbaoying, Liaoning Province (Shi et al., 2004). (g) $^{40}Ar/^{39}Ar$ and U-Pb ages from Jiaolai Basin (Li et al., 2023).~~

Formatado: Inglês (Estados Unidos)

Formatado: Centralizado

Formatado: Inglês (Estados Unidos)

6. Conclusions

Contrary to earlier hypotheses that associated CORBs with very low sedimentation rates, this study reveals that accumulation rates at ODP Site 1049 possibly ranged from 0.5 to 0.9 cm/kyr during ~~the~~ Aptian-Albian times. These values demonstrate that CORBs can form under moderately low but not necessarily exceptionally slow sedimentation conditions, suggesting that other environmental or climatic factors also played a ~~more~~ significant role in their deposition. Temporal synchrony exists between Aptian CORB-related events in the Tethys and North Atlantic, reflecting their response to global cooling and sustained thermohaline circulation~~Temporal synchrony exists between CORB-related events in the Tethys and North Atlantic. Aptian CORBs reflect a response to global cooling and sustained thermohaline circulation~~. The onset of long-term Aptian CORBs, such as CORB 1 in the Tethys and CORB A in the North Atlantic, is best explained by global climatic cooling that promoted ~~and intensified~~ thermohaline circulation during the Aptian "Cold Snap." This cooling episode, likely initiated by the emplacement of LIPs and subsequent organic carbon burial during OAEs, promoted oxygenation of deep waters. These sustained oxic conditions, rather than high productivity, facilitated the widespread ~~deposition~~ formation of red beds. Unlike the longer-lasting Aptian CORBs, the Albian red beds are shorter in duration and exhibit clear orbital pacing. This suggests that Albian CORB deposition was more sensitive to high-frequency climatic oscillations and regional variability, reflecting a shift in the dominant environmental controls on red bed formation during this interval. Near the Aptian–Albian boundary, incomplete stratigraphic records linked to the OAE 1b event are common, complicating global correlations of this interval. Our astrochronological findings support recent evidence that ~2.4 Myr grand cycles also produced global hiatuses at the Aptian–Albian boundary, potentially biasing correlations of deep-water sections spanning ~114.5 to 111.9 Ma.

Data availability

All data used here is public and can be accessed on the website http://deepseadrilling.org and https://mlp.ldeo.columbia.edu/logdb/scientific_ocean_drilling. DSDP and ODP data can be accessed at https://web.iodp.tamu.edu/OVERVIEW/.

Author contribution

J.M.F.R.: conceptualization, methodology, validation, cyclostratigraphic analyses, astronomical tuning, and writing. J.F.S.: conceptualization, methodology, validation, and investigation, writing, project administration, and funding acquisition. D.R.F.: methodology, validation, cyclostratigraphic and astronomical tuning analyses, writing. M.F.: writing. F.F.: conceptualization, and writing. R.C.: conceptualization and writing.

Competing interests

The authors declare that they have no conflict of interest.

Acknowledgements

This study was financially supported by the Specialization and Postgraduate Program of Petrobras. J.M.F.RAMOS thanks Petrobras for Ph.D. process. The authors greatly acknowledge the review efforts of Mark Leckie, Helmut Weissert, and the anonymous reviewer.

Financial support

The paper is a part of the projects Processamento e interpretação de dados magnetoestratigráficos do Cretáceo das Bacias Brasileiras and Magneto-cicloestratigrafia do Cretáceo na Margem Equatorial Brasileira (MEQ), both financed by Petróleo Brasileiro S.A.—Petrobras (FAURGS 8368 and 8892). J.F.S. also thanks CNPq for grants #304022/2018–7 and #311231/2021–7. D.R.F. thanks the Foundation Carlos Chagas Filho Research Support of the State of Rio de Janeiro (FAPERJ–grant #E-26/200.931/2022) and CNPq (grant #314462/2020-1).

References

Ahmerkamp, S., Winter, C., Krämer, K., de Beer, D., Janssen, F., Friedrich, J., Kuypers, M. M. M., & Holtappels, M.: Regulation of benthic oxygen fluxes in permeable sediments of the coastal ocean, Limnol. Oceanogr., 62, 1–14, https://doi.org/10.1002/lno.10379, 2017.

Formatado: Português (Brasil)

Arthur, M., Dean, W. & Pratt, L.: Geochemical and climatic effects of increased marine organic carbon burial at the Cenomanian/Turonian boundary, Nature, 335, 714–717, https://doi.org/10.1038/335714a0, 1988.

Baksi, A. K.: Petrogenesis and timing of volcanism in the Rajmahal flood basalt province, northeastern India, Chem. Geol., 121, 73–90, https://doi.org/10.1016/0009-541(94)00124-Q, 1995.

Benson, W. E., Sheridan, R. E., Pastouret, L., Enos, P., Freeman, T., Murdrnaa, I.O., Worstell, P., Gradstein, F., Schmidt, R.R., Weaver, F.M. et Stuermer, D.H.: Init. Rep. Deep-Sea Drill.Proj., 44:1005 pp, 1978.

Berggren, W. A. and Van Couvering, J. A.: The Cenozoic and Mesozoic stages and their boundaries, Bull. Geol. Soc. Am., 85, 713–725, 1974.

Bottini, C., and Erba, E.: Mid-Cretaceous paleoenvironmental changes in the western Tethys, Clim. Past, 14, 1147–1163, 2018.
Bralower, T. J., Sliter, W. V., Arthur, M., R. Leckie, R. M., Allard, D., Schlanger, S. O.: Dysoxic/Anoxic Episodes in the Aptian-Albian (Early Cretaceous), The Mesozoic Pacific: Geology, Tectonics, and Volcanism, Volume 77, https://doi.org/10.1029/GM077p0005, 1993.

Breheret, J. G.: The mid-cretaceous organic-rich sediments from the Vocontian zone of the French southeast basin. In A. Mascle (Ed.), Hydrocarbon and petroleum geology of France. Special publication of the European association of petroleum geoscientists, No. 4, 295–320. Springer, 1994.

Browning, E. L. and Watkins, D. K.: Elevated Primary Productivity of Calcareous Nannoplankton Associated with Ocean Anxoic Event 1b during the Aptian/Albian Transition (Early Cretaceous), Papers in the Earth and Atmospheric Sciences, 237, https://digitalcommons.unl.edu/geosciencefacpub/237, 2008.

Channell, J. E. T., Freeman, R., Heller, F., & Lowrie, W.: Timing of diagenetic hematite growth in red pelagic limestones from Gubbio (Italy), Earth Planet. Sci. Lett., 58, 189–201, 1982.

Coccioni, R., Jovane, L., Bancalà, G., Bucci, C., Fauth, G., Frontalini, F., Janikian, L., Savian, J., Paes de Almeida, R., Mathias, G. L., & Trindade, R. I. F.: Umbria-Marche Basin, Central Italy: A reference section for the Aptian–Albian interval at low latitudes, Sci. Dril., 13, 42–46, https://doi.org/10.2204/iodp.sd.13.07.2011, 2012.

Coccioni, R., Sabatino, N., Frontalini, F., Gardin, S., Sideri, M., & Sprovieri, M.: The neglected history of Oceanic Anoxic Event 1b: insights and new data from the Poggio le Guaine section (Umbria–Marche Basin), Stratigraphy, 11, 245–282, 2014.
Coffin and , M. F. and Eldholm, O.: Large igneous provinces: Crustal structure, dimensions, and external consequences, Reviews of Geopysics, Volume 32, Issue 1, 1-36, https://doi.org/10.1029/93RG02508, 1994.

Duarte, D., Erba, E., Bottini, C., Wagner, T., Aduomahor, B., Jones, T. D., Nicholson, U.: Early Cretaceous deep-water bedforms west of the Guinea Plateau revise the opening history of the Equatorial Atlantic Gateway, Global and Planetary Change, 249, 104777, ISSN 0921-8181, https://doi.org/10.1016/j.gloplacha.2025.104777, 2025.

Dummann, W., Hofmann, P., Herrle, J. O., Frank, M., Wagner, T.: The early opening of the Equatorial Atlantic gateway and the evolution of Cretaceous peak warming. Geology 51, 476–480, 2023.

Dutkiewicz, A., Boulila, S., & Müller, R. D.: Deep-sea hiatus record reveals orbital pacing by 2.4 Myr eccentricity grand cycles, Nat. Commun., 15, 1998, 2024.

Erbacher, J., Huber, B. T., Norris, R. D., and Markey, M.: Increased thermohaline stratification as a possible cause for an ocean anoxic event in the Cretaceous period, Nature, 409, 18–21, 2001.

Formatado: Espaçamento entre linhas: simples

Eren, M., & Kadir, S.: Colour genesis of Upper Cretaceous pelagic red sediments within the Eastern Pontides, NE Turkey, Yerbilimleri, 24, 71–79, 2001.

Fauth, G., Krahl, G., Kochhann, K. G. D., Hünnig Bom, M. H., Baecker-Fauth, S., Bruno, M. D. R., da Silva dos Santos, A., Ceolin, D., Villegas-Martín, J., Strohschoen Jr., O., Savian, J. F., Leandro, C. G., de Mello, R. G., & de Oliveira Lima, F. H. O.: Astronomical calibration of the latest Aptian to middle Albian in the South Atlantic Ocean, Palaeogeogr. Palaeoclimatol. Palaeoecol., 602, 111175, https://doi.org/10.1016/j.palaeo.2022.111175, 2022.

Fischer, A. G., and Arthur, M. A.: Secular variations in the pelagic realm, SEPM Spec. Publ., 25, 19–50, 1977.

Friedrich, O., Norris, R. D., & Erbacher, J.: Evolution of middle to Late Cretaceous oceans — a 55 My record of Earth's temperature and carbon cycle, Geology, 40, 107–110, 2012.

Friedrich, O., J. Erbacher, K. Moriya, P. A. Wilson, and H. Kuhnert.: Warm saline intermediate waters in the Cretaceous tropical Atlantic Ocean, Nat. Geosci., 1, 453–457, 2008.

Gale, A. S., Mutterlose, J., & Batenburg, S.: The Cretaceous period, in Gradstein, F. M., Ogg, J. G., Schmitz, M. D., & Ogg, G. M. (Eds.), The Geologic Time Scale 2020, Elsevier, 1023–1068, 2020.

Gambacorta, G., Bersezio, R., Weissert, H., and E. Erba, E.: Onset and demise of Cretaceous oceanic anoxic events: The coupling of surface and bottom oceanic processes in two pelagic basins of the western Tethys, Paleoceanography, 31, 732–757, doi:10.1002/ 2015PA002922, 2016.

Gilder, S., Chen, Y., Cogne, J. P., Tan, X. D., Courtillot, V., Sun, D. J., & Li, Y. A.: Paleomagnetism of Upper Jurassic to Lower Cretaceous volcanic and sedimentary rocks from the western Tarim Basin …, Earth Planet. Sci. Lett., 206, 587–600, https://doi.org/10.1016/S0012-821X(02)01074-9, 2003.

Giorgioni, M., et al.: Paleoceanographic changes during the Albian–Cenomanian in the Tethys and North Atlantic and the onset of the Cretaceous chalk, Glob. Planet. Change, 126, 46–61, 2015.

Giorgioni, M., Tiraboschi, D., Erba, E., Hamann, Y., Weissert, H..: Sedimentary patterns and palaeoceanography of the Albian Marne a Fucoidi Formation (Central Italy) revealed by high-resolution geochemical and nannofossil data, Sedimentology, 64, 111–126, 2017.

Haq, B. U., Hardenbol, J. and Vail, P. R.: Chronology of Fluctuating Sea Levels since the Triassic. Science, 235, 1156-1167, http://dx.doi.org/10.1126/science.235.4793.1156, 1987.

Hay, W. W.: Evolving ideas about the Cretaceous climate and ocean. Cretaceous Research, v. 29, p. 725–753, 2008.
Hay, W. W.: Cretaceous oceans and ocean modeling. From: SEPM Society for Sedimentary Geology 91, Cretaceous Oceanic Red Beds: Stratigraphy, Composition, Origins, and Paleoceanographic and Paleoclimatic Significance: ISBN 978-1-56576-135-3, 243–271, 2009.

Herbert, T. D., Stallard, R. E, and Fischer, A. G.: Anoxic Events, Productivity and Rhythms, and the Orbital Signature in a mid-Cretaceous deep-sea sequence from Central Italy, Paleoceanography, 1,495–506, 1986.

Herrle, J. O., Kossler, P., Friedrich, O., Erlenkeuser, H., & Hemleben, C.: High-resolution carbon isotope records of the Aptian to lower Albian from SE France and the Mazagan Plateau (DSDP site 545): A stratigraphic tool for paleoceanographic and paleobiologic reconstruction. Earth and Planetary Science Letters, *218*(1–2), 149–161. https://doi.org/10.1016/S0012-821X(03)00646-0, 2004.

Formatado: Espaçamento entre linhas: simples

Herrle, J. O., Schroder-Adams, C. J., Davis, W., Pugh, A. T., Galloway, J. M., & Fath, J.: Mid-cretaceous High Arctic stratigraphy, climate, and oceanic anoxic events. Geology, 43(5), 403–406. https://doi.org/10.1130/G36439.1, 2015.

Hochuli, E: North Gondwanan Floral Elements in Lower to Middle Cretaceous Sediments of the Southern Alps (Southern Switzerland, Northern Italy)', *Review of Paleobotany and Palynology* 35,337–358, 1981.

Hu, X., Jansa, L., and Sarti, M.: Mid-Cretaceous oceanic red beds in the Umbria-Marche Basin, central Italy: constraints on paleoceanography and paleoclimate, Palaeogeogr. Palaeoclimatol. Palaeoecol., 233, 163–186, 2005a.

Hu, X. M., Wang, C. S., Li, X. H., & Jansa, L.: Upper Cretaceous oceanic red beds in southern Tibet: lithofacies, environments and colour origin, Sci. China Ser. D – Earth Sci., 49, 785–795, 2006b.

Hu, X., Scott, R. W., Cai, Y., Wang, C., Melinte-Dobrinescu, M. C.: Cretaceous oceanic red beds (CORBs): different time scales and models of origin, Earth Sci. Rev., 115, 217–248, 2012.

Huber, B. T., MacLeod, K. G.,Gröcke, D., and Kucera, M.: Paleotemperature and paleosalinity inferences and chemostratigraphy across the Aptian/Albian boundary in the subtropical North Atlantic, Paleoceanography, v. 26, p. PA4221, 2011.

Huber, B. T., and Leckie, M. R.: Planktic foraminiferal species turnover across deep-sea Aptian/Albian Boundary sections, Journal of Foraminiferal Research, 41, 53–95, 2011.

Huber, B. T., MacLeod, K. G., Watkins, D. K., and Coffin, M. F.: The rise and fall of the Cretaceous Hot Greenhouse climate, Glob. Planet. Change, 167, 1–23, 2018.

Jansa, L. and Hu, X.: Cretaceous Pelagic Black Shales and Red Beds in Western Tethys: Origins, Paleoclimate, and Paleoceanographic Implications. 10.2110/sepmsp.091.059, 2009.

Kemper, E.; Das Klima der Kreidezeit, Geol. Jb., A96, 5-185, 1987.

Kochhann, K. G. D., Huber, B. T., Holbourn, A. E., and Kuhnt, W..: Benthic foraminiferal response to the Aptian–Albian carbon cycle perturbation in the Atlantic Ocean, J. Foraminiferal Res., 53, 214–225, 2023.

Krassilov, V. A.: Climatic changes in Eastern Asia as indicated by fossil floras. I. Early cretaceous, Palaeogeography, Palaeoclimatology, Palaeoecology, 13, Issue 4, 261-273, ISSN 0031-0182, https://doi.org/10.1016/0031-0182(73)90028-X, 1973.

Lam, A. R., Suganuma, Y., Kuroda, J., Hasegawa, T. and O'Regan, M.: Diachroneity rules the mid-latitudes: a test case using late Neogene planktic foraminifera across the Western Pacific, Geosciences, 12, 1–43, 2022.

Larson, R. L.: Geological consequences of superplumes, Geology, 19, 963–966, 1991.

Larson, R. L., & Erba, E.: Onset of the mid-Cretaceous greenhouse in the Barremian-Aptian: Igneous events and the biological, sedimentary, and geochemical responses. Paleoceanography, 14(6), 663–678. https://doi.org/10.1029/1999PA900040,1999.

Laskar, J., Robutel, P., Joutel, F., Gastineau, M., Correia, A., and Levrard, B.: A long-term numerical solution for the insolation quantities of the Earth, Astron. Astrophys., 428, 261–285, https://doi.org/10.1051/0004-6361:20041335, 2004.

Laskar, J.: Astrochronology. In Geologic time scale 2020,139–158, 2020.

Formatado: Espaçamento entre linhas: simples

Formatado: Português (Brasil)

Leandro, C. G., Savian, J. F., Kochhann, M. V. L., Franco, D. R., Coccioni, R., Frontalini, F., Gardin, S., Jovane, F., Figueiredo, M., Tedeschi, L. R., Janikian, L., Almeida, R. P., & Trindade, R. I. F.: Astronomical tuning of the Aptian stage and its implications for age recalibrations and paleoclimatic events, Nat. Commun., 13, 2941, https://doi.org/10.1038/s41467-022-30075-3, 2022.

Leckie, R. M.: A paleoceanographic model for the early evolutionary history of planktonic foraminifera, Palaeogeography, Palaeoclimatology, Palaeoecology, 73, Issues 1–2, 107-138, ISSN 0031-0182, https://doi.org/10.1016/0031-0182(89)90048-5, 1989.

Leckie, R. M., Bralower, T. J. and Cashman, R.: Oceanic anoxic events and plankton evolution: biotic response to tectonic forcing during the mid-Cretaceous. Paleoceanography, 17, 13–1 to 13–29. doi: 10.1029/2001PA000623, 2012.

Li, M., Hinnov, L., and Kump, L.: Acycle: time-series analysis software for paleoclimate research and education, Comput. Geosci., 127, 12–22, https://doi.org/10.1016/j.cageo.2019.02.011, 2019.

Li, X., Hu, X., Cai, Y., and Han, Z.: Quantitative analysis of iron oxide concentrations within Aptian–Albian cyclic oceanic red beds in ODP Hole 1049C, North Atlantic, Sediment. Geol., 235, 91–99, 2011.

Li, Y., Singer, B. S., Takashima, R, Schmitz, M. D., Podrecca, L. G., Sageman, B. B., Selby, D. Yamanaka, T., Mohr, M. T., Hayashi, K., Tomaru, T., Savatic, K.: Radioisotopic chronology of Ocean Anoxic Event 1a: Framework for analysis of driving mechanisms. Sci. Adv. 10, eadn8365, 2024.

Liu, S., Hernández-Molin, F. J., Rodrigues, S. and Rooij, D. V.: Deep-water circulation in the northeast Atlantic during the mid- and Late Cretaceous, Geology, 51 (6): 515–520, https://doi.org/10.1130/G50886.1, 2023.

Li, Y., Qin, H., Jicha, B. R., Huyskens, M. H. et al.: Revised onset age of magnetochron M0r: Chronostratigraphic and geologic implications: Geology, v. 51, p. 565, 2023.

Matsumoto, H., Minoshima, K., Yamaguchi, K., & Ishikawa, T.: Mid-Cretaceous marine Os isotope evidence for heterogeneous causes of oceanic anoxic events, Nat. Commun., 13, 239, 2022.

Mann, M. E., and Lees, J. M.: Robust estimation of background noise and signal detection in climatic time series, Clim. Change, 33, 409–445, 1996.

McAnena, A., Flögel, S., Hofmann, P., Herrle, J.O., Griesand, A., Pross, J., Talbot, H.M., Rethemeyer, J. and Wagner, T.: Atlantic cooling associated with a marine biotic crisis during the mid-Cretaceous period, Nat. Geosci., 6, 558–561, 2013.

MacLeod, K. G., Huber, B. T., Pletsch, T., T, Röhl, U. and Kucera, M.: Maastrichtian foraminiferal and paleoceanographic changes on Milankovitch timescales, Paleoceanography, 16, 2, 133–154, 2001.

Meyers, S. R., Sageman, B., and Hinnov, L.: Integrated quantitative stratigraphy of the Cenomanian–Turonian Bridge Creek Limestone Member using evolutive harmonic analysis and stratigraphic modeling, J. Sediment. Res., 71, 627–643, 2001.

Norris, R. D., Kroon, D., Klaus, A., et al.: Proceedings of the Ocean Drilling Program, Initial Reports, Vol. 171B, 1998.

O'Brien, C. L., Lear, C. H., & Wade, B. S.: Cretaceous sea-surface temperature evolution: constraints from TEX86 and planktonic foraminiferal oxygen isotopes, Earth Sci. Rev., 172, 224–247, 2017.

Ogg, J. G., and Bardot, L.: Aptian through Eocene magnetostratigraphic correlation of the Blake Nose Transect (Leg 171B), Florida continental margin, in Kroon, D., Norris, R. D., & Klaus, A. (Eds.), Proc. ODP, Sci. Results, 171B, 1–58, 2001.

Formatado: Espaçamento entre linhas: simples

Ogg, J.G., Röhl, U., and Geib, T., :Astronomical tuning of Aptian–Albian boundary interval: oceanic anoxic event OAE 1b through Lower Albian magnetic polarity subchron M″-2r.″, Eos, 80:F491–492, 1999.

Percival L. M. E., Matsumoto, H., Callegaro, S., Erba, E., Kerr, A. C., Mutterlose, J. and Suzuki, K.: Cretaceous large igneous provinces: from volcanic formation to environmental catastrophes and biological crises, in: Cretaceous Project 200 Volume 1: the Cretaceous World, edited by: Hart, M. B., Batenburg, S. J., Huber, B. T., Price, G. D., Thibault, N., Wagreich, M. and Walaszczyk, I., Geological Society, London, Special Publications, 544, https://doi.org/10.1144/SP544-2023-88, 2024.

Petrizzo, M. R.: Late Cretaceous planktonic foraminiferal bioevents in the Tethys and in the Southern Ocean record: an overview, J. Foraminiferal Res., 33, 330–337, 2003.

Premoli Silva, I., Erba, E. and Tornaghi, M.E.: Paleoenvironmental signals and changes in surface fertility in mid Cretaceous Corg-Rich pelagic facies of the Fucoid Marls (Central Italy). Geobios, 22, 225–236, 1989.

Ramos, J. M. F. Savian, J. F., Franco, D. R., Figueiredo, M. F., Leandro, C. G., Frontalini, F., et al.: Astronomical calibration of the Ocean Anoxic Event 1b and its implications for the cause of mid-Cretaceous events: a multiproxy record, Paleoceanogr. Paleoclimatol., 39, e2024PA004860, https://doi.org/10.1029/2024PA004860, 2024a.

Ramos, J. M. F., Savian, J. F., Franco, D. R., Figueiredo, M. F., Leandro, C. G., & Frontalini, F.: Orbital tuning of short reversed geomagnetic polarity intervals in the Cretaceous Normal Polarity Superchron, Geophys. Res. Lett., 51, e2024GL110530, https://doi.org/10.1029/2024GL110530, 2024b.

Ramos, J.M.F., Savian, J.F., Franco, D. R. et al.: New insights into the early opening of the Equatorial Atlantic Gateway revealed through a magneto-cyclostratigraphy framework from the Brazilian Equatorial Margin. Commun. Earth Environ., **6**, 958, https://doi.org/10.1038/s43247-025-02910-0, 2025.

Ryan, W. B. F., Bolli, H. M., Foss, G. N., Natland, J. H., Hottman, W. E., and Foresman, J. B.: Objectives, principle results, operations, and explanatory notes of Leg 40, South Atlantic. In Bolli, H.M., Ryan, W.B.F., et al., Init. Repts. DSDP, 40: Washington (U.S. Govt. Printing Office), 5–26, 1978.

Ryan, W. B. E and Cita, M. B.: Ignorance Concerning Episodes of Ocean-Wide Stagnation, Marine Geology 23, 197–215 , 1977.

Santos, A., Mota, M. A. L. Kern, H. P., Fauth, G. et al.: Earlier onset of the Early Cretaceous Equatorial humidity belt. Glob. Planet. Change 208, 1–14, 2022.

Savin, S. M.: The History of the Earth's Surface Temperature During the Last 100 Million Years, Annual Reviews of Earth and Planetary Science, 5, 319-355, 1977.

Savian, J. F., Trindade, R. I. F., Janikian, L., Jovane, L., Almeida, R. P., Coccioni, R., et al.: The Barremian-Aptian boundary in the Poggio le Guaine core (central Italy): Evidence for magnetic polarity Chron M0r and oceanic anoxic event 1a. *Geological Society of America Special Paper*, *524*, 57–78. https://doi.org/10.1130/2016.2524(05), 2016.

Schlanger, S. O., and H. C. Jenkyns.: Cretaceous oceanic anoxic events: Causes and consequence, Geol. Mijnbouw, 55(3–4), 179–184, 1976.

Shi, R., He, H., Zhu, R., & Pan, Y.: ISEA reversed event in the Cretaceous normal superchron (CNS): $^{40}Ar/^{39}Ar$ dating and paleomagnetic results, Chin. Sci. Bull., 49, 926–930, https://doi.org/10.1007/bf03184013, 2004.

Formatado: Espaçamento entre linhas: simples

Sinninghe Damsté, J. S., and Köster, J. A.: A euxinic southern North Atlantic Ocean during the Cenomanian/Turonian oceanic anoxic event, Earth Planet. Sci. Lett., 158, 165–173, 1998.

Steinig, S., Dummann, W., Hofmann, P., Frank, M., Park, W., Wagner, T., and Flögel, S.: Controls on Early Cretaceous South Atlantic Ocean circulation and carbon burial – a climate model–proxy synthesis, Clim. Past, 20, 1537–1558, https://doi.org/10.5194/cp-20-1537-2024, 2024.

Tarduno, J. A.: Brief reversed polarity interval during the Cretaceous Normal Polarity Superchron, Geology, 18, 683–686, https://doi.org/10.1130/0091-7613(1990)018<0683:BRPIDT>2.3.CO;2, 1990.

Tarduno, J. A., Sliter, W. V., Kroenke, L., Leckie, M., Mayer, H., Mahoney, J. J., et al.: Rapid Formation of Ontong Java plateau by Aptian mantle Plume volcanism. Science, 254(5030), 399–403. https://doi.org/10.1126/science.254.5030.399, 1991.

Tarduno, J. A., Lowrie, W., Sliter, W. V., Bralower, T. J., & Heller, F.: Reversed polarity characteristic magnetizations in the Albian Contessa sections, Umbrian Apennines, Italy: Implications for the existence of a Mid-Cretaceous mixed polarity interval. Journal of Geophysical Research, 97(B1), 241–271. https://doi.org/10.1029/91jb02257, 1992.

Tiraboschi, D., Coccioni, R., Jovane, F., and Frontalini, F.: Origin of rhythmic Albian black shales (Piobbico core, central Italy): calcareous nannofossil quantitative and statistical analyses and paleoceanographic reconstructions, Paleoceanography, 24, PA4206, 2009.

Thomson, D. J.: Spectrum estimation and harmonic analysis, Proc. IEEE, 70, 1055–1096, 1982.

Trabucho Alexandre, J., Gilst, R. I. V., Rodriguez-Lopez, J. P., De Boer, P. L.: The sedimentary expression of oceanic anoxic event 1b in the North Atlantic, Sedimentology, 58, 1217–1246, 2011.

VandenBerg, J., Klootwijk, C. T., and Wonders, A. A. H.: The late Mesozoic and Cenozoic movements of the Umbrian Peninsula: further paleomagnetic data from the Umbrian sequence, Geol. Soc. Am. Bull., 89, 133–155, 1978.

Waltham, D.: Milankovitch Period Uncertainties and their Impact on cyclostratigraphy, Journal of Sedimentary Research, 85(8), 990–998, https://doi.org/10.2110/jsr.2015.66, 2015.

Wang, C., Hu, X., Jansa, L., Li, X., & Wang, S.: Upper Cretaceous oceanic red beds in southern Tibet: a major change from anoxic to oxic, deep-sea environments, Cretac. Res., 26, 21–32, 2005.

Wang, C., Hu, X., Scott, R. W., Wagreich, M., & Jansa, L.: Overview of Cretaceous Oceanic Red Beds (CORBs): a window on global oceanic and climate change, in Cretaceous Oceanic Red Beds: Stratigraphy, Composition, Origins, and Paleoceanographic and Paleoclimatic Significance, SEPM Spec. Publ. 91, 13–33, 2009.

Weissert, H. and McKenzie, J. A.: Anoxic Sediments in the Early Cretaceous Tethys Ocean: An Oceanographic Explanation, International Association of Sedimentologists, European Meeting, Abstracts, 205 – 207, 1981.

Weissert, H., McKenzie, J. A., and Channell, J. E. T.: Natural Variations in the Carbon Cycle During the Early Cretaceous', in E. T. Sundquist and W. S, Broecker (eds.), The Carbon Cycle and Atmospheric C02: Natural Variations Archean to the Present, American Geophysical Union, Geophysical Monograph, 32, pp. 531–545, 1985.

Weissert, H.: C-Isotope stratigraphy, a monitor of paleoenvironmental change: A case study from the early cretaceous. Surveys in Geophysics, 10, 1–61, https://ui.adsabs.harvard.edu/abs/1989SGeo...10....1W, 1989.

Formatado: Espaçamento entre linhas: simples

Formatado: Inglês (Estados Unidos)

Weissert, H., Lini, A., Föllmi, K. B., and Kuhn, O.: Correlation of Early Cretaceous carbon isotope stratigraphy and platform drowning events: a possible link?, Palaeogeogr. Palaeoclimatol. Palaeoecol., 137, 189–203, 1998.

Yamamoto, A., Abe-Ouchi, A., Shigemitsu, M., Oka, A., Takahashi, K., Ohgaito, R., & Yamanaka, Y.: Global deep ocean oxygenation by enhanced ventilation in the Southern Ocean under long-term global warming, Glob. Biogeochem. Cycles, 29, 1801–1815, https://doi.org/10.1002/2015GB005181, 2015.

Zhang, D., Yan, M., Song, C., Zhang, W., Fang, X., & Li, B.: Frequent polarity reversals in the Cretaceous Normal Superchron, Geophys. Res. Lett., 48, 2020GL091501, https://doi.org/10.1029/2020GL091501, 2021.

Ahmerkamp, S., et al. Regulation of benthic oxygen fluxes in permeable sediments of the coastal ocean. Limnology and Oceanography 62(1), 1-14, 2017.

Arthur, M. A., Brumsack, H. J., Jenkyns, H. C., & Schlanger, S. O. In. Cretaceous Resources, Events and Rhythms, 75-119, 1990.

Erba, E. et al. Environmental consequences of Ontong Java Plateau and Kerguelen Plateau volcanism. In The origin, evolution, and environmental impact of oceanic large igneous provinces. Geol. Soc. Am. Spec. Pap. 511, 2015

Baksi, A. K. Petrogenesis and timing of volcanism in the Rajmahal flood basalt province, northeastern India. Chemical Geology, 121(1-4), 73-90, https://doi.org/10.1016/0009-541(94)00124-Q, 1995.

Berggren, W. A., and Van Couvering, J. A. The Cenozoic and Mesozoic stages and their boundaries". Bulletin of the Geological Society of America 85(5), 713-725, 1974.

Bice, K. L., Barron, E. J. & Peterson, W. H. Continental runoff and early Cenozoic bottom-water sources. Geology 25, 951-954, 1997.

Bottini, C. & Erba, E. Mid-Cretaceous paleoenvironmental changes in the western Tethys. Clim. Past 14, 1147-1163, 2018.

Boulila, S. Coupling between grand cycles and events in Earth's climate during the past 115 million years. Sci. Rep. 9, 327, 2019.

Channell, J.E.T., Freeman, R., Heller, F., Lowrie, W. Timing of diagenetic hematite growth in red pelagic limestones from Gubbio (Italy). Earth and Planetary Science Letters 58, 189-201, 1982.

Coccioni, R. et al. Umbria-Marche Basin, Central Italy: A Reference Section for the Aptian-Albian Interval at Low Latitudes. Sci. Drill. 13, 42-46, 2012.

Coccioni, R. et al. The neglected history of Oceanic Anoxic Event 1b: insights and new data from the Poggio le Guaine section (Umbria-Marche Basin). Stratigraphy 11, 245-282, 2014.

Dossmann, P. M., et al. Mixing and Formation of Layers by Internal Wave Forcing. Journal of Geophysical Research: Oceans 122(12), 10,038-10,057, 2017.

Dutkiewicz, A., Boulila, S., Müller, R. D. Deep-sea hiatus record reveals orbital pacing by 2.4Myr eccentricity grand cycles. Nature Communications, 15:1998, 2024.

Eldhom, O. and M Coffin, M. F. Large Igneous Provinces and Plate Tectonics, in: The History and Dynamics of Global Plate Motions, edited by: Mark A. Richards, Richard G. Gordon, Rob D. Van Der Hilst. Geophysical Monograph Series. American Geophysical Union, 309-326, https://doi.org/10.1029/GM121p0309.

Erbacher, J., Thurow, J. & Littke, R. Evolution patterns of radiolaria and organic matter variations - a new approach to identify sea-level changes in mid-Cretaceous pelagic environments. Geology 24, 499-502, 1996.

Erbacher, J. et al. Increased thermohaline stratification as a possible cause for an ocean anoxic event in the Cretaceous period. Nature 409(18), 2001.

Eren, M. and Kadir, S. Colour genesis of Upper Cretaceous pelagic red sediments within the Eastern Pontides, NE Turkey. Yerbilimleri 24, 71-79, 2001.

Fauth, G. et al. Astronomical calibration of the latest Aptian to middle Albian in the South Atlantic Ocean. Palaeogeography, Palaeoclimatology, Palaeoecology 602, 111175, 2022.

Fearon, J. D., et al. Enhanced Vertical Mixing in Coastal Upwelling Systems Driven by Diurnal-Inertial Resonance: Numerical Experiments. Journal of Geophysical Research: Oceans, 125(6), e2020JC016208, 2020.

Fischer, A. G. & Arthur, M. A. Secular variations in the pelagic realm. SEPM Spec. Publ. 25, 19-50, 1977.

Formatado: Espaçamento entre linhas: simples

Formatado: Espaçamento entre linhas: simples

Friedrich, O., Norris, R. D. & Erbacher, J. Evolution of middle to Late Cretaceous oceans—a 55 my record of Earth's temperature and carbon cycle. Geology 40, 107–110, 2012.

Gale, A. S., Mutterlose, J. & Batenburg, S. In Geologic Time Scale 2020, (eds. Gradstein, F. M., Ogg, J. G., Schmitz, M. D., Ogg, G. M.) 1023–1068, 2020.

Gilder, S., Chen, Y., Cogne, J. P., Tan, X. D., Courtillot, V., Sun, D. J., & Li, Y. A. Paleomagnetism of Upper Jurassic to Lower Cretaceous volcanic and sedimentary rocks from the western Tarim Basin and implications for inclination shallowing and absolute dating of M-0 (ISEA?) chron. Earth and Planetary Science Letters, 206 (3–4), 587–600, https://doi.org/10.1016/S0012-821X(02)01074-9, 2003.

Giorgioni, M. et al. Paleoceanographic changes during the Albian–Cenomanian in the Tethys and North Atlantic and the onset of the Cretaceous chalk. Glob. Planet. Chang. 126, 46–61, 2015.

Hu, X. et al. Upper Cretaceous oceanic red beds (CORBs) in the Tethys: occurrences, lithofacies, age, and environments. Cretaceous Research 26, 3–20, 2005a.

Hu, X., Jansa, L., and Sarti, M. Mid-Cretaceous oceanic red beds in the Umbria-Marche Basin, central Italy: Constraints on paleoceanography and paleoclimate. Palaeogeography, Palaeoclimatology, Palaeoecology, 233, 163–186, doi: 10.1016/j.palaeo.2005.10.003, 2005b.

Hu, X.M., Jansa, L., Sarti, M. Mid-Cretaceous oceanic red beds in the Umbria-Marche Basin, central Italy: constraints on paleoceanography and palaeoclimate. Palaeogeography, Palaeoclimate, Palaeoecology 233, 163–186, 2006a.

Hu, X.M., Wang, C.S., Li, X.H., Jansa, L. Upper Cretaceous oceanic red beds in southern Tibet: lithofacies, environments and colour origin. Science in China Series D-Earth Sciences 49, 785–795, 2006b.

Hu, X. et al. Cretaceous oceanic red beds (CORBs): Different time scales and models of origin. Earth-Science Reviews 115, 217–248, 2012.

Huber, B. T. et al. Paleotemperature and paleosalinity inferences and chemostratigraphy across the Aptian/Albian boundary in the subtropical North Atlantic. Paleoceanography 26, PA4221 (2011). doi:10.1029/2011PA002178

Huber, B. T., MacLeod, K. G., Watkins, D. K. & Coffin, M. F. The rise and fall of the Cretaceous Hot Greenhouse climate. Glob. Planet. Change 167, 1–23, 2018.

Jenkyns, H. C. Mesozoic anoxic events and paleoclimate. Zbl. Geol. PalaÈont. Teil 1. 7-9, 943-949, 1997.

Thurow, J., Brumsack, H. J., RullkoÈtter, J. & Meyers, P. The Cenomanian/Turonian Boundary Event in the Indian Ocean : a key to understand the global picture. Geophys. Monogr. 70, 253–273, 1992.

Kochhann, K. G. D. et al. Benthic Foraminiferal Response to the Aptian–Albian Carbon Cycle Perturbation in the Atlantic Ocean. Journal of Foraminiferal Research 53(3), 214–225, 2023.

Kocken, I. J., Cramwinckel, M. J., Zeebe, R. E., Middelburg, J. J. & Sluijs, A. The 405 kyr and 2.4 Myr eccentricity components in Cenozoic carbon isotope records. Clim. Past 15, 91–104, 2019.

Lam, A. R. et al. Diachroneity Rules the Mid-Latitudes: A Test Case Using Late Neogene Planktic Foraminifera across the Western Pacific. Geosciences 12, 1-43, 2022.

Larson, R. L. Geological consequences of superplumes. Geology 19, 963–996, 1991.

Laskar, J., Robutel, P., Joutel, F., Gastineau, M., Correia, A., & Levrard, B. A long-term numerical solution for the insolation quantities of the Earth. Astronomy & Astrophysics, 428(1), 261–285, https://doi.org/10.1051/0004-6361:20041335, 2004.

Leandro, C. G., Savian, J.F., Kochhann, M.V.L., Franco, D.R., Coccioni, R., Frontalini, F., Gardin, S., Jovane, F., Figueiredo, M., Tedeschi, L.R., Janikian, L., Almeida, R.P., Trindade, R.I.F. Astronomical tuning of the Aptian stage and its implications for age recalibrations and paleoclimatic events. Nat. Commun. 13, 2941, https://doi .org /10 .1038 /s41467-022-30075-3, 2022.

Li, X. et al. Quantitative analysis of iron oxide concentrations within Aptian–Albian cyclic oceanic red beds in ODP Hole 1049C, North Atlantic. Sedimentary Geology 235, 91–99, 2011.

Li, M., Hinnov, L., Kump, L. Acycle: Time-series analysis software for paleoclimate research and education. Comput. Geosci. 127, 12–22, https://doi.org/10.1016/j.cageo.2019.02.011, (2019).

Matsumoto, H. et al. Mid-Cretaceous marine Os isotope evidence for heterogeneous cause of oceanic anoxic events. Nat. Commun. 13, 239, 2022.

Mann, M. E., Lees, J. M. Robust Estimation of Background Noise and Signal Detection in Climatic Time Series. Climatic Change, Vol. 33, pp. 409-445, 1996.

Código de campo alterado

McAnena, A. et al. Atlantic cooling associated with a marine biotic crisis during the mid-cretaceous period. Nat. Geosci. 6 (7), 558–561, 2013.

Meyers, S. R., Sageman, B., Hinnov, L. Integrated quantitative stratigraphy of the Cenomanian-Turonian Bridge Creek Limestone Member using evolutive harmonic analysis and stratigraphic modeling, J. Sediment. Res., 71, 627–643, 2001.

Norris, R. D., Kroon, D., Klaus, A., et al., Proceedings of the Ocean Drilling Program, Initial Reports, Vol. 171B, 1998.

O'Brien, C. L. et al. Cretaceous sea-surface temperature evolution: constraints from TEX86 and planktonic foraminiferal oxygen isotopes. Earth Sci. Rev. 172, 224–247, 2017.

Ogg, J. G., and Bardot, L. Aptian through Eocene magnetostratigraphic correlation of the Blake Nose Transect (Leg 171B), Florida continental margin. In Kroon, D., Norris, R.D., and Klaus, A. (Eds.), Proc. ODP, Sci. Results, 171B, 1–58, 2001.

Olsen, P. E. et al. Mapping solar system chaos with the Geological Orrery. Proc. Natl Acad. Sci. USA 116, 10664–10673, 2019.

Overview of Cretaceous Oceanic Red Beds (CORBs): a Window on Global Oceanic and Climate Change. Wang, C. et al. From: SEPM Society for Sedimentary Geology 91, Cretaceous Oceanic Red Beds: Stratigraphy, Composition, Origins, and Paleoceanographic and Paleoclimatic Significance: 13–33, 2009.

Petrizzo, M. R. Late Cretaceous planktonic foraminiferal bioevents in the Tethys and in the Southern Ocean record: an overview. Journal of Foraminiferal Research 33(4), 330–337, 2003.

Ramos. J. M. F. Astronomical Calibration of the Ocean Anoxic Event 1b and Its Implications for the Cause of Mid-Cretaceous Events: A Multiproxy Record. Paleoceanography and Paleoclimatology 39, e2024PA004860, 2024a.

Ramos, J. M. F., Savian, J. F., Franco, D. R., Figueiredo, M. F., Leandro, C. G., & Frontalini, F. Orbital tuning of short reversed geomagnetic polarity intervals in the Cretaceous Normal Polarity Superchron. Geophysical Research Letters 51, e2024GL110530, https://doi. org/10.1029/2024GL110530, 2024b.

Rovelli, L., et al. Thermocline mixing and vertical oxygen fluxes in the stratified central North Sea. Biogeosciences 13(5), 1609–1624, 2016.

Ryan, W. B., Bolli, H. M., Foss, G. N., Natland, J. H., Hottman, W. E., & Foresman, J. B. Objectives, principal results, operations and explanatory notes of Leg 40, South Atlantic. Initial reports of the deep sea drilling project, 40, 5–28, 1978.

Savian, J. F., Trindade, R. I. F., Janikian, L., Jovane, L., Almeida, R. P., Coccioni, R., et al. The Barremian-Aptian boundary in the Poggio le Guaine core (central Italy): Evidence for magnetic polarity Chron M0r and oceanic anoxic event 1a. Geological Society of America Special Paper 524, 57–78, https://doi.org/10.1130/2016.2524(05), 2016.

Schlanger, S. O. & Jenkyns, H. C. Cretaceous oceanic anoxic events: causes and consequences. Geol. en. Mijnb. 55, 179–184, 1976.

Shi, R., He, H., Zhu, R., & Pan, Y. ISEA reversed event in the cretaceous normal Super-chron (CNS): 40Ar/39Ar dating and paleomagnetic results. Chinese Science Bulletin, 49(9), 926–930, https://doi.org/10.1007/bf03184013, 2004.

Sinninghe Damsté, J. S. & Köster, J. A euxinic southern North Atlantic Ocean during the Cenomanian/Turonian oceanic anoxic event. Earth Planet. Sci. Lett. 158, 165–173, 1998.

Tarduno, J. A. Brief Reversed Polarity Interval during the Cretaceous normal Polarity Superchron. Geology 18 (8), 683–686. doi:10.1130/0091-7613(1990)018<0683:brpidt>2.3.co;2, 1990.

Tiraboschi, D. et al. Origin of rhythmic Albian black shales (Piobbico core, central Italy): Calcareous nannofossil quantitative and statistical analyses and paleoceanographic reconstructions: Paleoceanography 24, 2009.

Thomson, D.J. Spectrum estimation and harmonic analysis. Proc. IEEE 70,1055–1096, 1982.

VandenBerg, J., Klootwijk, C.T., and Wonders, A.A.H. The late Mesozoic and Cenozoic movements of the Umbrian Peninsula: Further paleomagnetic data from the Umbrian sequence: Geological Society of America Bulletin 89 133–155, 1978.

Vail, P. R. et al. Seismic stratigraphy and global changes of sea level, in Payton, C. E., ed., Seismic Stratigraphy Application to Hydrocarbon Exploration: Tulsa, American Association of Petroleum Geologists Memoir 26, p. 49–205, 1977.

Wang, C. et al. Upper Cretaceous oceanic red beds in southern Tibet: a major change from anoxic to oxic, deep-sea environments Cretaceous Research 26, 21–32, 2005.

Yamamoto, A., A. Abe-Ouchi, M. Shigemitsu, A. Oka, K. Takahashi, R. Ohgaito, and Y. Yamanaka. Global deep ocean oxygenation by enhanced ventilation in the Southern Ocean under long-term global warming, Global Biogeochem. Cycles 29, 1801–1815, doi:10.1002/2015GB005181, 2015.

Wang, J., et al. Benthic Respiration in Hypoxic Waters Enhances Bottom Water Acidification in the Northern Gulf of Mexico. Journal of Geophysical Research: Oceans 125(7), e2020JC016152, 2020.

Wang, C. et al. "Overview of Cretaceous Oceanic Red Beds (CORBs): a window on global oceanic and climate change." In X. Hu, C. Wang, R. W. Scott, M. Wagreich, & L. Jansa (Eds.), Cretaceous Oceanic Red Beds: Stratigraphy, Composition, Origins, and Paleoceanographic and Paleoclimatic Significance. Special publication / Society for Sedimentary Geology, pp. 13-33, 2009.

Weissert, H., Lini, A., FoÈllmi, K. B. & Kuhn, O. Correlation of Early Cretaceous carbon isotope stratigraphy and platform drowning events: a possible link? Palaeogeogr. Palaeoclim. Palaeecol. 137, 189-203, 1998.

Zhang, D., Yan, M., Song, C., Zhang, W., Fang, X., & Li, B. Frequent polarity reversals in the Cretaceous Normal Superchron. Geophysical Research Letters 48, 2020GL091501, https://doi.org/10.1029/2020GL091501, 2021.